GROUND-MOTION RELATIONS FOR HARD ROCK SITES IN EASTERN NORTH AMERICA

Gail M. Atkinson
Dept. Earth Sciences, Carleton University
Ottawa, Ontario K1A 5B6
613-623-3240 (phone/fax)
gmatkinson@aol.com

Final Technical Report:
USGS Award 02HQGR0001
Dec. 1, 2004

Ground-Motion Relations for Hard Rock Sites in Eastern North America

Gail M. Atkinson

Final Technical Report: USGS Award 02HQGR0001. Dec. 1, 2004

ABSTRACT

New earthquake ground-motion relations for hard-rock sites in eastern North America (ENA) are presented based on a stochastic finite-fault model. The model incorporates new information obtained from ENA seismographic data gathered over the last 10 years, including 3-component broadband data. The effects of epistemic uncertainty in model parameters and aleatory uncertainty (variability) on the median predictions are evaluated. The new relations are not dramatically different from the previous relations of Atkinson and Boore (1995), which were based on a stochastic point-source model. The relations agree well with available ENA ground motion data over a broad range of magnitudes and distances.

INTRODUCTION

A decade has passed since Atkinson and Boore (1995) developed their ground-motion relations for eastern North America. The Atkinson and Boore (1995) relations (AB95) were based on a stochastic point-source methodology (Boore, 1983), with the model source and attenuation parameters determined from empirical data from small to moderate earthquakes in eastern North America (ENA). Specifically, the AB95 model rested heavily on the two-corner source spectral model of Atkinson (1993a) and the spectral attenuation model of Atkinson and Mereu (1992).

Since 1995, there have been several advancements that make it timely to develop new ENA ground motion relations:

1. An additional 10 years of ground-motion data have been gathered, including broadband data that extend the bandwidth of ENA ground motion databases (Atkinson, 2004) and improve the definition of attenuation trends within 100 km of the source.
2. New analyses demonstrate that attenuation in ENA in the first 70 km is faster than previously believed. The geometric spreading rate is $R^{-1.3}$, where R is hypocentral distance (Atkinson, 2004). The new attenuation has a significant impact on predicted ground motions.
3. Stochastic finite-fault modeling techniques that can be used to develop regional ground motion relations for both point sources and large faults have been extended and validated (Beresnev and Atkinson, 1997, 2001; Motazedian and Atkinson, 2005). It has also been demonstrated that a point-source model can mimic the salient effects of finite-fault models through appropriate specification of an equivalent point source representation (Atkinson and Silva, 2000). As a

result of developments in stochastic modeling, it is now feasible to use a finite fault model to improve ground-motion predictions for larger earthquakes in ENA.

In this report, new ENA ground-motion relations for hard-rock sites are presented based on a stochastic finite-fault model. The effects of epistemic uncertainty in model parameters and aleatory uncertainty (variability) are evaluated. The stochastic finite-fault model predictions are compared to the previous point-source predictions of Atkinson and Boore (1995). Complementary to this report, point-source models of ENA ground-motion are also being updated; the finite-fault and point-source models are compared to each other, and to ENA data, in order to develop a full suite of predictive equations (Atkinson and Boore, 2005). The results presented herein are a preliminary and abbreviated version of the Atkinson and Boore (2005) ground-motion relations.

METHODOLOGY AND MODEL PARAMETERS

Ground-motion relations are developed for response spectra (pseudo-acceleration, 5% damped), peak ground acceleration (PGA) and peak ground velocity (PGV), for hard-rock sites in ENA (near-surface shear-wave velocity $\beta > 2$ km/s), as a function of moment magnitude and closest distance to the fault rupture. For seismic hazard analysis, we are primarily interested in ground motions from earthquakes of moment magnitude (**M**) > 5, at distances less than 100 km from the source. Because of the paucity of recorded ENA ground motions in this magnitude-distance range, it is not feasible to develop ENA ground-motion relations directly from regression analysis of empirical data. Rather, ENA ground-motion relations are derived from a simulated ground-motion database. The simulated ground motions are developed from a seismological model of source, path and site parameters. For this study, the seismological model parameters are obtained using empirical data from small to moderate ENA earthquakes. The methodology itself is validated by application to other data-rich regions (California). Finally, the model predictions are compared to the available ENA ground-motion database.

The simulations to develop the ENA ground-motion relations are based on the well-known stochastic method. In our previous relations (Atkinson and Boore, 1995), a stochastic point-source model was used. In the current work, we employ a stochastic finite-fault model to better include significant finite fault effects such as the geometry of larger ruptures and its effects on attenuation, and directivity. The simulations are performed with the computer code EXSIM (Motazedian and Atkinson, 2005). This code is an updated version of the well-known FINSIM stochastic finite-fault model code (Beresnev and Atkinson, 1997; 2001). The EXSIM code differs from FINSIM in conceptual improvements that treat subfault parameters more dynamically, making the simulations independent of subfault size, and allowing slip pulses to be shorter than the duration of fault rupture (similar to the self-healing slip model of Heaton, 1990).

Stochastic Simulation Model

The stochastic model is a widely-used tool to simulate acceleration time series and develop ground-motion relations (Hanks and McGuire, 1981; Boore, 1983; Atkinson

and Boore, 1995 and 1997; Toro et al., 1997; Atkinson and Silva, 2000). The stochastic method begins with the specification of the Fourier spectrum of ground motion as a function of magnitude and distance. Typically the acceleration spectrum is modeled by a spectrum with an ω^2 shape, where ω = angular frequency (Aki, 1967; Brune, 1970, 1971; Boore 1983). The "Brune model" spectrum is derived for an instantaneous shear dislocation at a point. The acceleration spectrum of the shear wave, A(f), at hypocentral distance R from an earthquake is given by:

$$A(f) = CM_0 (2\pi f)^2 / [1+ f/ f_0)^2] \exp(-\pi f \kappa) \exp(-\pi f R/Q\beta)/R \quad (1)$$

where M_0 is seismic moment and f_0 is corner frequency, which is given by $f_0 = 4.9*10^6 \beta (\Delta\sigma / M_0)^{1/3}$ where $\Delta\sigma$ is stress drop in bars, M_0 is in dyne-cm, and β is shear wave velocity in km/s (Boore, 1983). The constant $C = \Re^{\theta\varphi} F V /(4\pi\rho\beta^3)$, where $\Re^{\theta\varphi}$ = radiation pattern (average value of 0.55 for shear waves), F= free surface amplification (2.0), V= partition onto two horizontal components (0.71), ρ= density, and R= hypocentral distance (Boore, 1983). The term $\exp(-\pi f \kappa)$ is a high-cut filter to account for near-surface "*kappa*" effects, which describe the commonly observed rapid spectral decay at high frequencies (Anderson and Hough, 1984). In the above equation the power of R in the denominator of the attenuation term, $\exp(-\pi f R/Q\beta)/R$, is considered equal to 1, which is appropriate for body-wave spreading in a whole space. This value can be changed as needed in order to account for deviations from 1/R due to factors such as postcritical reflections from the Moho discontinuity or multiply reflected waves traveling in the crustal waveguide. The quality factor, $Q(f)$, is an inverse measure of anelastic attenuation . Through this equation, the spectrum is diminished with distance to account for empirically-defined attenuation behavior.

Finite fault modeling has been an important tool for the prediction of ground motion near the epicenters of large earthquakes (Hartzell, 1978; Irikura, 1983; Joyner and Boore, 1986; Heaton and Hartzell, 1986; Somerville et al., 1991; Tumarkin and Archuleta, 1994; Zeng et al., 1994; Beresnev and Atkinson, 1998a). One of the most useful methods to simulate ground motion for a large earthquake is based on the simulation of a number of small earthquakes as subfaults that comprise an extended fault plane. A large fault is divided into N subfaults and each subfault is considered as a small point source (introduced by Hartzell, 1978). Ground motions of subfaults, each of which may be calculated by the stochastic point-source method as described above, are summed with a proper time delay in the time domain to obtain the ground motion from the entire fault, a(t):

$$a(t) = \sum_{i=1}^{nl} \sum_{j=1}^{nw} a_{ij}(t + \Delta t_{ij}) \quad (2)$$

where *nl* and *nw* are the number of subfaults along the length and width of main fault, respectively (*nl*nw* = N), and Δt_{ij} is the relative time delay for the radiated wave from the ij^{th} subfault to reach the observation point. The $a_{ij}(t)$ are each calculated by the stochastic point source method (Boore, 1983).

The stochastic method has also been used to derive ground-motion relations for many different regions. Atkinson and Boore (1995) derived ground-motion relations for eastern North America, using a stochastic point-source model with an empirical two-corner source model. Toro *et al.* (1997) developed similar relations for eastern North America using a Brune point-source model. Atkinson and Silva (2000) developed ground-motion relations for California using a stochastic method that exploits the equivalence between the finite fault model and a two-corner point-source model of the earthquake spectrum. In each of these cases, region-specific input parameters derived from seismograms were used to specify the model parameters that drive the ground-motion relations for that region. For California, where there is a good empirical strong-motion database, it was shown that the stochastic relations agree well with empirical regression equations (e.g. Abrahamson and Silva, 1997; Boore et al., 1997; Sadigh et al., 1997). The stochastic ground-motion relations provide a sound basis for estimating peak ground motions and response spectra for earthquakes of magnitude 4 through 8, at distances from 1 to 200 km over the frequency range 0.2 to 20 Hz.

In this study, we use a stochastic finite-fault approach. A modified version of the computer program FINSIM (Beresnev and Atkinson, 1998b) was used for the simulations. The modifications to FINSIM introduce the new concept of a "dynamic corner frequency" to more closely model real finite-fault dynamic behavior. The method is presented in Appendix A. The modified program has been renamed EXSIM (Extended earthquake fault simulation program). EXSIM model parameters that represent the earthquake source processes have been calibrated for general applications, using data from 27 moderate to large well-recorded earthquakes in California (Motazedian and Atkinson, 2005). For use in ENA, the model requires region-specific attenuation and generic site parameters, which are derived from recordings of small-to-moderate earthquakes.

EXSIM is used to simulate a ground-motion database from which to develop ground-motion equations. We take this approach because there are not enough real data in the magnitude-distance ranges of engineering interest (**M** 5 to 7.5 at distances less than 200 km). We can use the empirical data to establish the underlying parameters and validate the model predictions. The region-specific parameters needed for simulations are:

1. Attenuation of Fourier amplitudes with distance (geometric spreading and Q-value).
2. Duration of ground motion as a function of magnitude and distance.
3. Regional generic crust/site amplifications and physical constants.
4. Source parameters for simulation: stress drop, and pulsing percentage. The stress drop controls the amplitudes of high-frequency radiation, while the percentage of the fault that is pulsing at any time (simulating healing behavior as the rupture front passes) controls the relative amount of low-frequency radiation.

With these parameters established, we can use the calibrated EXSIM model to extend our predictions to the magnitude-distance range of interest. We then compare predictions with ENA data.

Model Parameters for Simulations and their Uncertainty

The input model parameters for ENA ground motion simulations are defined as discussed below. For parameters with significant uncertainty, we consider the effects of epistemic and aleatory uncertainty, where epistemic uncertainty reflects our uncertainty concerning the true median value of the parameter, and aleatory uncertainty expresses random variability in the parameter from one ground-motion realization to another (Toro and McGuire, 1987).

In the simulations to produce median ground-motion relations, we include epistemic uncertainty by treating each key parameter as a probability distribution, with the given median value and some uncertainty about that median. Normal or random distributions are used to express the uncertainty, depending on the parameter being modeled. When simulating epistemic uncertainty, we consider only the uncertainty in the median value (not its random variability from one realization to the next). To examine aleatory uncertainty, the same approach and same median parameter values are used, except in this case the probability distributions are broader, to reflect the random fluctuations in the actual effective values of the parameters that are observed from one ground motion record to another.

To give an example, the median value for stress drop in our simulations is 140 bars, based on the analysis of apparent source spectra from 35 ENA events of **M**≥4 (Table 4). The log of the stress drop is a normally distributed parameter (mean log stress = 2.14) with standard deviation 0.31 log units (factor of 2 variability), and standard error of the mean (epistemic uncertainty) of 0.05 log units. Thus epistemic uncertainty in stress drop is modeled using a normal distribution of log stress with mean 2.14 and standard deviation 0.05, while its aleatory uncertainty is modeled with mean 2.14 and standard deviation 0.31.

In the presentation of model parameters below, the median parameters are explained, along with the models used to represent epistemic and aleatory uncertainty. Table 1 summarizes the median parameter values, while Tables 2 and 3 present the epistemic and aleatory uncertainties, respectively. Uncertainty is included only for the key parameters that have a significant impact on predicted amplitudes. Other parameters, such as physical constants, are modeled with fixed parameter values.

Attenuation of Fourier amplitudes with distance

The attenuation of spectral amplitudes in ENA has recently been studied using a database of 1700 recordings of small to moderate ENA events recorded on hard-rock sites (Atkinson, 2004). This empirical study is a significant update of previous empirical models of attenuation (Atkinson and Mereu, 1992), including 10 more years of seismographic data, and incorporating newer 3-component broadband data. The new analysis reveals that geometric spreading is significantly faster at near-source distances (<70 km) than was determined in previous studies. Specifically, Fourier amplitudes decay as $R^{-1.3}$ within 70 km of the source, then increase as $R^{+0.2}$ in the distance range from 70 km to 140 km (due to Moho bounce effects), then decrease as $R^{-0.5}$ at R>140 km. The associated Q model is given by $Q = 893\ f^{0.32}$ with a minimum Q of 1000 (Atkinson, 2004). This attenuation model is used to diminish spectral amplitudes of subsource radiation with distance from the earthquake source.

Uncertainty in the rates of attenuation, and their effects on amplitudes at distance, is best modeled by considering uncertainty in the geometric spreading coefficient, which is of most significance. In this study, based on detailed evaluation of the regression results of Atkinson (2004), the epistemic uncertainty in attenuation is modeled by normal distributions considering the geometric spreading coefficient in the first 70 km to be given by -1.3±0.1, and in the transition zone (70 to 140 km) by +0.2±0.2. This range of coefficients propagates attenuation uncertainty to larger distances (>140 km), and is sufficient to model the net effects of uncertainty in all attenuation parameters. (Note that attenuation uncertainties are coupled, such that uncertainties in geometric spreading and Q cannot be treated as independent.) Aleatory uncertainty provides a broader scatter of effective attenuation parameters from one event to the next, and is modeled as a random distribution, with the range of spreading coefficient being -1.5 to -1.1 in the first 70 km, and -0.5 to +0.9 in the transition zone (note these ranges result in the median values of -1.3 and +0.2, respectively).

Atkinson (2004) found that the attenuation in ENA depends slightly on the focal depth of the earthquake, and proposed depth-correction factors to the attenuation model based on depth. These factors were included in the simulations, according to the event's focal depth (depth is discussed below under 'Source Parameters'). These depth correction factors to the attenuation are a relatively insignificant component of the overall attenuation, and their uncertainty is not modeled; rather it is considered part of the overall attenuation uncertainty modeled through the assumed variability in geometric spreading rates.

Duration of Ground Motion

The duration (T) of an earthquake signal at hypocentral distance R can generally be represented as (Atkinson and Boore, 1995):

$$T(R) = T_0 + dR \qquad (3)$$

where T_0 is the source duration, and d is the coefficient controlling the increase of duration with distance; d is derived empirically. d may be a single coefficient describing all distances of interest (eg. Atkinson, 1993b), or it can take different values depending on the distance range (eg. Atkinson and Boore, 1995). The empirical duration model of Atkinson and Boore (1995) was adopted for this study. The duration increases in a hinged trilinear fashion from the source, mimicking the trilinear form of the attenuation model. The coefficients for d are 0.16, -0.03 and 0.04, for the distance ranges 0 to 70 km, 70-130 km, and >130 km, respectively (see Atkinson and Boore, 1995). The source duration is estimated as the subfault rise time, as determined by the subfault radius and the rupture propagation speed. We re-examined this duration model in light of recent data, and saw no evidence that this model should be revised. The uncertainty in duration is not modeled, as it is less significant than uncertainty in other parameters in terms of its impact on simulated ground motion amplitudes.

Regional generic crust/site amplifications and physical constants

The shear-wave velocity (β) at average focal depths (near 13 km) is assumed to be 3.7 km/s, with density (ρ) 2.8 g/cm^3. These are typical regional values (Boore and Joyner, 1997). Shear-wave velocity actually depends on depth, so in the modeling of

alternative focal depths (discussed below), the value of β is selected based on the event depth, such that β increases from a value of 3.1 km/s at a depth of 5 km, through the value 3.7 at 13 km, to a maximum of 3.8 km/s for depths of 14.5 km or more. These values were based on typical crustal shear-wave velocity profiles (eg. Somerville et al., 2003). The physical constants are not a significant source of uncertainty.

Amplification of horizontal-component ground motions, for rock sites, occurs due to the combined effects of the velocity gradient in the crust, and near-surface amplification due to the weathered layer of rock in the top few meters. (There is additional site response for soil sites, but this is not the subject of this study; rock motions can be modified to model soil sites by adding these additional soil amplifications.) An approximation of the amount of amplification may be obtained empirically using the H/V ratios (horizontal-to-vertical component ratios) for rock sites in ENA, as discussed by Atkinson (2004). The basic idea is that amplification of the vertical component is very small compared to that of the horizontal component, allowing H/V to provide a first-order site amplification estimate (Lermo and Chavez-Garcia, 1993; Siddiqqi and Atkinson, 2002). The assumed amplification for ENA rock sites increases from a value of 1.0 for frequencies less than 0.5 Hz, to a value of 1.41 at f≥10 Hz, as given by Siddiqqi and Atkinson (2002).

Variability in site amplification is modeled by using an additional randomly-drawn amplification factor ranging from -0.15 to +0.15 log units for each trial. This uncertainty is applied in the representation of both epistemic uncertainty and variability. In the epistemic sense, it represents our uncertainty in actual rock amplification for an unknown rock site; if the response is better known for a particular site based on site-specific studies, then this value could be reduced and would reduce overall epistemic uncertainty (as per the sum of the squares addition rules for uncertainties). In the aleatory sense, this uncertainty represents the typical random variability that is seen even among nearby sites with apparently similar site conditions.

Amplification effects are counteracted at high frequencies by the effects of the kappa parameter (Anderson and Hough, 1984). Kappa acts to rapidly diminish spectral amplitudes above some frequency, and is believed to be primarily a site effect. For hard-rock sites in ENA, the effects of kappa are nearly negligible. Atkinson (1996) estimated a value of κ=0.002. In this study, a careful examination of the spectral data presented by Atkinson (2004) was made to search for evidence of the high-frequency shape factor. This indicated a minimum κ of 0, with a maximum value for individual records of 0.01. The aleatory uncertainty in κ is represented by a random distribution from 0.002 to 0.01, while its epistemic uncertainty is represented as a random variable from 0.002 to 0.006.

Source parameters for simulation

The most important source parameter for the simulations is the stress drop, which controls the spectral amplitudes at high frequencies. The distribution of this parameter was determined from the high-frequency level of apparent source spectra for all ENA events of **M**≥4, as listed in Table 4, at a reference distance of 20 km (denoted A_{hf}(20km)). The source spectra for instrumentally-recorded earthquakes were determined by using the attenuation model of Atkinson (2004) to correct all observations back to the reference distance of 20 km; the source spectrum of an event was obtained by

averaging the log amplitudes at this reference distance over all stations that recorded the event. The stress was then defined as the Brune stress drop value required to reproduce this high-frequency spectral level (the stress drop parameter in EXSIM is approximately equal to the point-source Brune stress drop). High-frequency spectral levels were also estimated for pre-instrumental events based on their felt area. As shown by Atkinson (1993a), the felt area of an earthquake is well correlated with high-frequency spectral level. The empirical relationship of Atkinson (1993a) between these two parameters was updated in this study to include all events through 2003 with both determined spectral levels and felt areas. The new relationship for A_{hf}(20km) based on felt area is shown in Figure 1 and given by:

$$\log A_{hf}(20\text{km}) = -4.78 + 0.92 \log \text{Afelt} \qquad (4)$$

where A_{hf}(20km) is in cm/s and Afelt is in km^2. This relationship was used in Table 4 to determine the stress drop for events having no modern instrumental data, but a well-determined felt area. In preparing Table 4, only events with a known moment magnitude (from independent studies) were considered, except for the 1811 New Madrid and 1886 Charleston events, which were assigned nominal moment magnitudes of 7.5 and 7.0, respectively (see Hough et al., 2000; Johnston, 1996). The stress drop values are plotted versus moment magnitude on Figure 2. Some studies have suggested a decrease in stress drop with increasing magnitude, at least for California (eg. as discussed in Atkinson and Silva, 2000). No such trend is apparent on Figure 2. Furthermore, the determination of a stress drop near 200 bars for the 2001 **M**7.7 Bhuj, India earthquake (Singh et al., 2004) argues against a decreasing stress drop trend for large intracontinental events.

Based on the data in Table 4, the median stress drop is 140 bars. Uncertainty in the median is represented by a normal distribution in log stress, with the inter-event variability in stress being represented by the standard deviation of log stress of 0.31 units (eg. factor of 2 variability in stress drop represents 1 standard deviation). The epistemic uncertainty in the median value is represented by the standard error of the mean log stress, which is 0.054 log units (eg. factor of 1.13 uncertainty in median stress).

The percentage pulsing area is taken as 25%, which means that at most 25% of the fault plane is slipping at any moment in time. This parameter is assumed based on calibration studies with California data (Motazedian and Atkinson, 2005). It is assigned a relatively large epistemic uncertainty, represented by a random distribution from 10% to 50%. The assumed aleatory variability is represented by a random distribution from10% to 90%. This parameter is not well known, but does not exert a large influence on the simulated amplitudes at most frequencies (it exerts a moderate influence at lower frequencies, as discussed by Motazedian and Atkinson, 2005).

Earthquake focal depths in ENA cover a broad range from a few km to 30 km. Recent depth determinations (Ma and Atkinson, 2005) were used to determine a mean focal depth of 13 km. Depth is assumed to be normally distributed. The epistemic uncertainty in mean depth is assumed to be 3 km, with an aleatory variability expressed by a standard deviation of 10 km (with an assumed minimum depth of 2 km, and maximum of 30 km).

Other source parameters that are considered uncertain include the fault dip, given by the mean value of 50 degrees, with epistemic and aleatory uncertainty of 10 degrees

and 20 degrees, respectively. The fault length and width, which are functions of magnitude, are also considered uncertain. EXSIM assumes the fault lengths and widths given by the global empirical relationships of Wells and Coppersmith (1994). However, recent data suggest that ENA fault dimensions are probably significantly smaller for a given moment magnitude (Somerville et al., 2003). This effect is modeled by multiplying the fault length and width obtained by the Wells and Coppersmith relations by a randomly distributed factor. The length factor ranges from 0.3 to 0.7, or 0.2 to 0.8, to represent epistemic and aleatory uncertainty in fault length, respectively, while the width factor ranges from 0.6 to 0.8 and 0.4 to 1.0 for epistemic and aleatory uncertainty, respectively. These factors do not have a significant impact on predicted amplitudes, except for very large events (**M**>7). The location of the hypocenter on the fault plane is assumed to be random, as is the slip distribution.

RESULTS

Simulations were performed using the EXSIM model with the median parameters as listed in Table 1, including epistemic uncertainty as given by the distributions in Table 2. Moment magnitudes from 3.5 to 8.0 were simulated, in 0.5 magnitude unit increments, at 24 values of fault distances ranging from 1 to 1000 km. A profile of 8 lines at equally spaced azimuths spreading out from the fault plane was used for each distance to capture the average effects of directivity. For each magnitude and observation point, 3 random trials were performed. Thus a total of 5760 horizontal-component ground motion records were simulated (10*24*8*3), all for rock sites. These records were used to compute 5% damped pseudo-acceleration spectra (PSA) as well as peak ground acceleration (PGA) and velocity (PGV).

Figure 3 plots response spectral amplitudes from the simulations versus closest distance to the fault; note that this figure includes the variability in amplitudes due to epistemic uncertainty, but not the total random variability expected due to aleatory uncertainty. The figure plots amplitudes for magnitudes 5, 6, 7 and 8, along with curves that represent the median amplitudes. The curves were determined by averaging log amplitudes within distance bins 0.1 log units in width for each magnitude value, then lightly smoothing these curves over distance with a 3-point triangular smoothing. The resulting values are given for all magnitudes from 3.5 to 8.0 in Table 5. These values represent preliminary median ground motion relations for ENA rock sites. Values for fault distances less than 10 km are obtained only for large events, since the focal depth effect means that small events will necessarily be some significant distance from observation points on the Earth's surface, while large events have sufficient fault width to rupture to the surface. (Just for the geometric purposes of placing the fault within the crust, it is assumed that the depth of the hypocenter is at the middle of the fault width; if this implies a surface rupture, the fault width extends from the surface to the depth indicated by the fault width and dip.)

We observe that these new relations are not dramatically different from the previous relations of Atkinson and Boore (1995), shown as dashed lines on Figure 3. The main difference is that high-frequency amplitudes are somewhat less for large-magnitude earthquakes, due to the improved consideration of finite-fault effects. The similarity of

the new relations to those of Atkinson and Boore (1995) is interesting, given the increase in database and new simulation methodology used in this study. It lends weight to previous conclusions that a two-corner point-source model can be used to mimic salient finite-fault effects in the development of ground motion relations (Atkinson and Silva, 2000).

Epistemic uncertainty in ground motion amplitudes appears to be independent of both magnitude and distance, as illustrated in Figure 4. It has an average value of 0.22 log units (factor of 1.66) for all frequencies. Thus our uncertainty in the correct median parameter values for the simulations implies our relations could be too high or low by a factor of about 1.7 (within 84% confidence limits). If the site amplification is known for a specific site (say to within 0.05 log units), the epistemic uncertainty might be reduced to about 0.20 log units (factor of 1.6). Further reduction in epistemic uncertainty is unlikely without significant improvements in knowledge of regional source and path effects.

Aleatory uncertainty was modeled by repeating the simulations using the aleatory parameters distributions of Table 3. This does not affect the median ground motions obtained, but results in greater scatter. Figure 5 shows the obtained aleatory variability, representing random scatter in ground motion amplitudes. The aleatory uncertainty is also independent of magnitude and distance, with an average value of 0.26 log units over all frequencies. There is a very slight tendency for aleatory variability to decrease with increasing frequency, from a value of 0.27 at 0.2 Hz to a value of 0.24 at 10 Hz; this trend may not be significant. This calculated variability, based purely on the simulation parameters, agrees remarkably well with typically observed values for empirical strong-ground motion relations in California (eg. Boore et al., 1993; Abrahamson and Silva, 1997).

Another way to address uncertainty in the ground motion relations, as well as their reliability, is to compare the predicted ground motions with observations. Table 6 lists response spectra data for rock sites in ENA, based on data presented by Atkinson and Boore (1998), Atkinson and Chen (1997) and Atkinson (2004). In addition, the Bhuj, India observations of Cramer and Kumar (2003) are included, corrected to hard-rock site conditions using the site condition factors of Adams and Halchuck (2003). The Bhuj data are included because of the suggested similarity of the Bhuj and New Madrid earthquakes (Cramer and Kumar, 2003; Bodin et al., 2004; Singh et al., 2004), but their relevance is less certain than that of the other data, particularly in light of the need to make site corrections to obtain equivalent values for hard-rock conditions.

All of the ENA data in Table 6 have been plotted on Figure 3 for a qualitative comparison with the ground-motion relations. Broadly speaking, the relations appear to be in reasonable agreement with the data, with two exceptions:

- The relations overpredict observations from **M**5 events at large distances.
- The relations underpredict a cluster of enhanced high-frequency amplitude data for **M**6 near 100 km. This cluster represents strong-motion observations from the **M**5.8 1988 Saguenay, Quebec earthquake, which had particularly strong high-frequency amplitudes (Boore and Atkinson, 1992). Interestingly the high-frequency amplitudes from the Saguenay

event are nearly as large as those for the Bhuj earthquake, despite the large difference in their magnitudes. The relations predict the Bhuj amplitudes quite well.

A quantitative evaluation of the agreement between the ground-motion relations and data can be made by examining residuals, where the residual is defined as residual = log(observed PSA) – log(predicted PSA). Figure 6 plots residuals as a function of magnitude and distance for selected frequencies. This confirms the overall agreement noted in Figure 3, although it can be observed that residuals develop a negative trend (overprediction) at large distances (>300 km). Considering the residuals within 300 km, the average residual is within 0.1 log units (25%), indicating good agreement between data and predictions. The computed aleatory variability, based on the standard deviation of residuals, increases with frequency from a value of 0.3 at low frequencies (0.2 to 0.5 Hz) to 0.4 at high frequencies (5 to 10 Hz). The data-based aleatory variability is somewhat larger than the expected aleatory variability based on the simulations (eg. about 0.25 in the simulations vs. 0.35 in the data), and has the opposite trend with frequency. This discrepancy can be partly attributed to lack of control over site conditions and data quality in the dataset. Overall, the results of the simulations and the data comparisons suggest an aleatory variability of about 0.26, independent of frequency.

CONCLUSIONS

Ground-motion relations for hard-rock sites in ENA have been developed using a stochastic finite-fault methodology. Preliminary values of the median relations are given in Table 5. They are associated with an epistemic uncertainty of approximately 0.22 log (base 10) units and a random variability of approximately 0.26 log units (independent of magnitude, distance and frequency). The new relations are not dramatically different from the previous relations of Atkinson and Boore (1995). The relations agree well with available ENA ground motion data over a broad range of magnitudes and distances.

STUDY PUBLICATIONS

The publications by Atkinson and Sonley (2003) and Atkinson (2004), cited below, were completed as part of this research program. The material presented in this report is being further developed and submitted to Bull. Seism. Soc. Am. as a co-authored publication with David M. Boore (UGSG), under a similar title (projected publication date 2005).

REFERENCES

Abrahamson, N. and W. Silva (1997). Empirical response spectral attenuation relations for shallow crustal earthquakes. Seism. Res. L., **68**, 94-127.

Adams, J., and Halchuk, S. (2003). Fourth generation seismic hazard maps of Canada: Values for over 650 Canadian localities intended for the 2005 National Building Code of Canada. Geological Survey of Canada Open File 4459 150 pp.

Aki, K. (1967). Scaling law of seismic spectrum, J. Geophys. Res. 72, 1217-1231.

Anderson, J. and S. Hough (1984). A model for the shape of the Fourier amplitude spectrum of acceleration at high frequencies. Bull. Seism. Soc. Am., **74**, 1969-1993.

Atkinson, G. (1993a). Source spectra for earthquakes in eastern North America. Bull. Seism. Soc. Am., **83**, 1778-1798.

Atkinson, G. (1993b). Notes on ground motion parameters for eastern North America: Duration and H/V ratio. Bull. Seism. Soc. Am., **83**, 587-596.

Atkinson, G. (1996). The high-frequency shape of the source spectrum for earthquakes in eastern and western Canada. Bull. Seism. Soc. Am., **86**, 106-112.

Atkinson, G. (2004). Empirical attenuation of ground motion spectral amplitudes in southeastern Canada and the northeastern United States. Bull. Seism. Soc. Am.,**94**, 1079-1095.

Atkinson, G., and D. Boore (1995). New ground motion relations for eastern North America. Bull. Seism. Soc. Am., **85**, 17-30.

Atkinson, G., and D. Boore (1997). Stochastic point-source modeling of ground motions in the Cascadia region. Seism. Res. L., **68**, 74-85.

Atkinson, G. and D. Boore (1998). Evaluation of models for earthquake source spectra in eastern North America. Bull. Seism. Soc. Am., **88**, 917-934.

Atkinson, G. and D. Boore (2005). Improved ground-motion relations for eastern North America. Bull. Seism. Soc. Am., manuscript in preparation.

Atkinson, G. and S. Chen (1997). Regional seismograms from historical earthquakes in southeastern Canada. Seism. Res. L., **68**, 797-807.

Atkinson, G. and R. Mereu (1992). The shape of ground motion attenuation curves in southeastern Canada. Bull. Seism. Soc. Am., **82**, 2014-2031.

Atkinson, G. and W. Silva (2000). Stochastic modeling of California ground motions. Bull. Seism. Soc. Am., **90**, 255-274.

Atkinson, G. and E. Sonley (2003). Ground motions from the 20 April, 2002 Au Sable Forks, NY earthquake. Seism. Res. L., **74**, 330-349.

Beresnev, I. and G. Atkinson (1997). Modeling finite fault radiation from the w^n spectrum. Bull. Seism. Soc. Am., **87**, 67-84.

Beresnev, I. and G. Atkinson (1998a). Stochastic finite-fault modeling of ground motions from the 1994 Northridge, California earthquake. I. Validation on rock sites. Bull. Seism. Soc. Am., **88**, 1392-1401.

Beresnev, I. and G. Atkinson (1998b). FINSIM - a FORTRAN program for simulating stochastic acceleration time histories from finite faults. Seism. Res. L., **69**, 27-32.

Beresnev, I. and G. Atkinson (2001). Source parameters of earthquakes in eastern and western North America based on finite-fault modeling. Bull. Seism. Soc. Am., **91**, submitted.

Bodin, P. and S. Horton (2004). Source parameters and tectonic implications of aftershocks of the M_w 7.6 Bhuj earthquake of January 26, 2001, Bull. Seism. Soc. Am., **94**, 818-827.

Boore, D. (1983). Stochastic simulation of high-frequency ground motions based on seismological models of the radiated spectra. Bull. Seism. Soc. Am., **73**, 1865-1894.

Boore, D. and G. Atkinson (1992). Source spectra for the 1988 Saguenay, Quebec earthquakes. Bull. Seism. Soc. Am., **82**, 683-719.

Boore, D. and W. Joyner (1997). Site amplifications for generic rock sites. Bull. Seism. Soc. Am., **87**, 327-341.

Boore, D. W. Joyner and T. Fumal (1997). Equations for estimating horizontal response spectra and peak acceleration from western North American earthquakes: A summary of recent work. Seism. Res. L., **68**, 128-153

Brune, J. (1970). Tectonic stress and the spectra of seismic shear waves from earthquakes. J. Geophys. Res., **75**, 4997-5009.

Brune, J. (1971). Correction. J. Geophys. Res., 76, 5002.

Cramer, C. and A. Kumar (2003). 2001 Bhuj, India earthquake engineering seismoscope recordings and eastern North America ground motion attenuation relations. Bull Seism. Soc. Am., **93**, 1390-1394.

Hanks, T. and R. McGuire (1981). The character of high-frequency strong ground motion. Bull. Seism. Soc. Am., **71**, 2071-2095.

Hartzell, S. (1978). Earthquake aftershocks as Green's functions. Geophys. Res. Letters, **5**, 1-14.

Heaton, T. (1990). Evidence for and implications of self-healing pulses of slip in earthquake rupture. Phys. Earth Planet. Interiors, **64**, 1-20.

Heaton, T., and S. Hartzell (1986). Source characteristics of hypothetical subduction earthquakes in the Northwestern United States. Bull. Seism. Soc. Am., **76**, 675-708.

Hough, S., J. Armbruster, L. Seeber and J. Hough (2000). On the Modified Mercalli Intensities and magnitudes of 1811-1812 New Madrid earthquakes. J. Geophys. Res., **105**, 839-864.

Irikura, K. (1983). Semi-empirical estimation of strong ground motions during large earthquakes. Bull. Disaster Prevention Res. Inst., Kyoto Univ., **33**, 63-104.

Johnston, A. (1996). Seismic moment assessment of earthquakes in stable continental regions. Geophys. J. Intl.: **124**, 381-414 (Part I); **125**, 639-678 (Part II); **126**, 314-344 (Part III).

Joyner, W. and D. Boore (1986). On simulating large earthquakes by Green's function additon of smaller earthquakes. In: Earthquake Source Mechanics. Maurice Ewing Volume 6. Geophys. Monogr. Am. Geophys. Union, **37**, 269-274.

Lermo, J. and F. Chavez-Garcia (1993). Site effect evaluation using spectral ratios with only one station. Bull. Seism. Soc. Am., **83**, 1574-1594.

Ma, S. and G. Atkinson (2005). Focal depth distribution for earthquakes with MN $\geq$ 2.8 in western Quebec, southern Ontario and northern New York. Bull. Seism. Soc. Am.,submitted.

Motazedian, D. and G. Atkinson (2005). Stochastic finite-fault model based on dynamic corner frequency. Bull. Seism. Soc. Am., **95**, in press.

Sadigh, K., C. Chang, J. Egan, F. Makdisi and R. Youngs (1997). Attenuation relationships for shallow crustal earthquakes based on California strong motion data. Seism. Res. L., **68**, 180-189.

Siddiqqi, J. and G. Atkinson (2002). Ground motion amplification at rock sites across Canada, as determined from the horizontal-to-vertical component ratio. Bull. Seism. Soc. Am., **92**, 877-884.

Singh, S., J. Pacheco, B. Bansal, X. Perez-Campos, R Dattatrayam and G. Suresh (2004). A source study of the Bhuj, India, earthquake of 26 January 2001 (M_w7.6). Bull. Seism. Soc. Am., **94**, 1195-1206.

Somerville, P., M. Sen and B. Cohee (1991). Simulations of strong ground motions recorded during the 1985 Michoacan, Mexico and Valparaiso, Chile, earthquakes. Bull. Seism. Soc. Am., **81**, 1-27.

Somerville, P., N. Collins, N. Abrahamson, R. Graves and C. Saikia (2003). Ground motion attenuation relations for the central and eastern United States. Report to U.S. Geological Survey (NEHRP). Draft Bull. Seism. Soc. Am. manuscript.

Toro, G., N. Abrahamson and J. Schneider (1997). Model of strong ground motion in eastern and central North America: Best estimates and uncertainties. Seism. Res. L., **68**, 41-57.

Toro, G. and R. McGuire (1987). Calculational procedures for seismic hazard analysis and its uncertainty in the eastern United States. Proc. Third Intl. Conf. Soil Dynamics and Earthquake Eng., Princeton, pp. 195-206.

Tumarkin, A. and R. Archuleta (1994). Empirical ground motion prediction. Annali Di Geofisica. 37, 1691-1720..

Wells, D. and K. Coppersmith (1994). New empirical relationships among magnitude, rupture length, rupture width, rupture area, and surface displacement. Bull. Seism. Soc. Am., **84**, 974-1002.

Zeng, Y., J. Anderson and G. Yu (1994). A composite source model for computing realistic synthetic strong ground motions. Geophys. Res. L., in press.

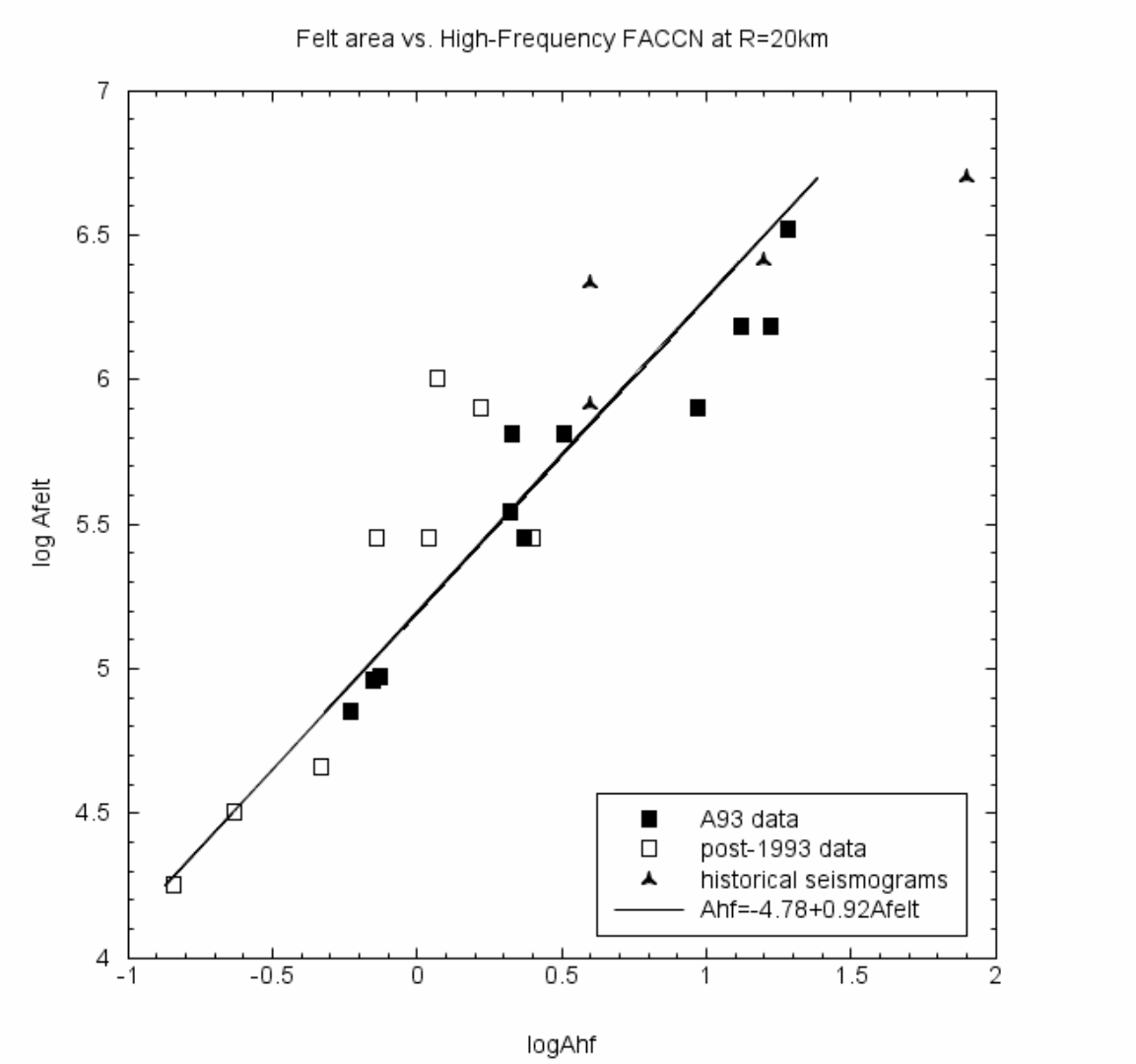

Figure 1 – Relationship between felt area and high-frequency spectral acceleration level (at a reference distance of 20 km). Symbols show data from Atkinson (1993a) (filled squares), new data from Atkinson (2004) (open squares) and historical seismogram data of Atkinson and Chen (1997). Lines show least-squares fit.

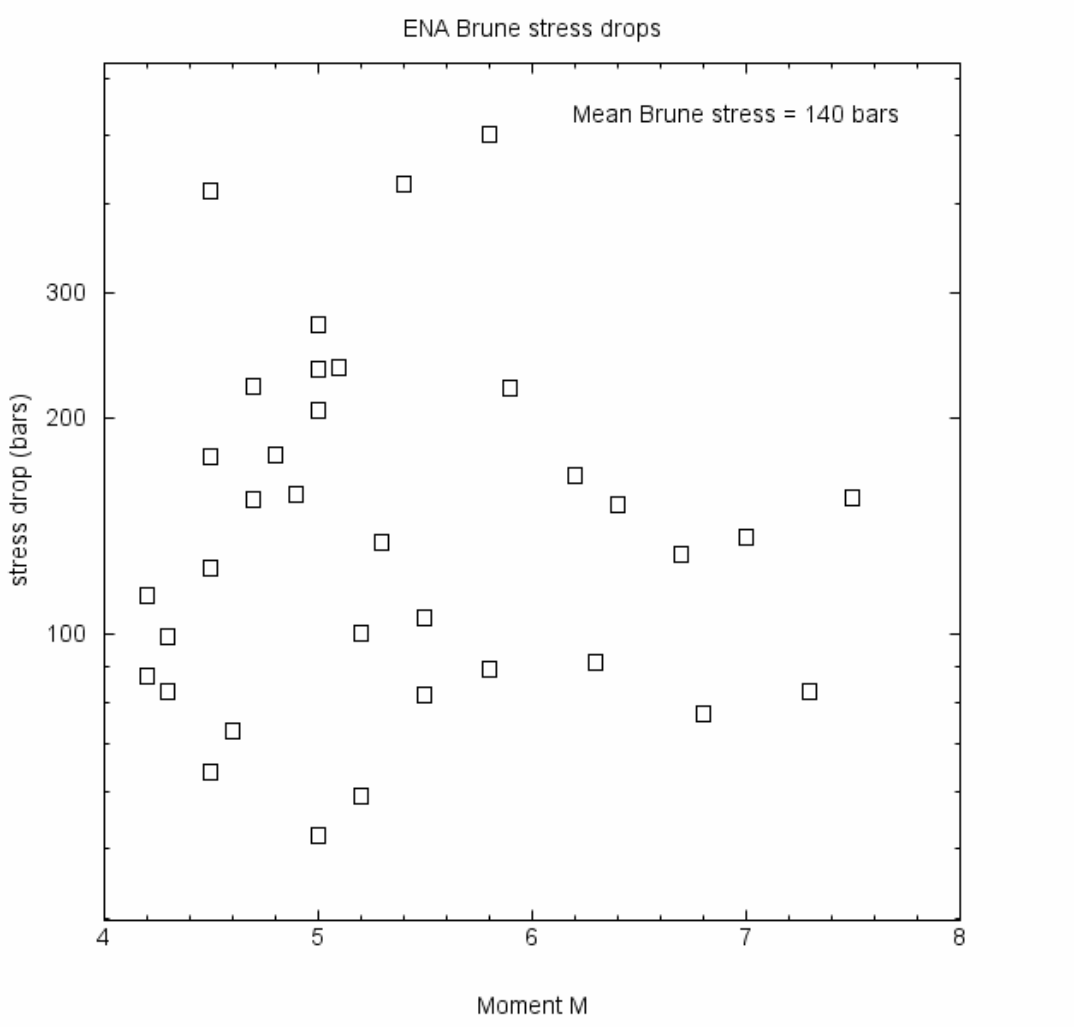

Figure 2 – ENA Brune stress drops (controlling high-frequency spectral level)

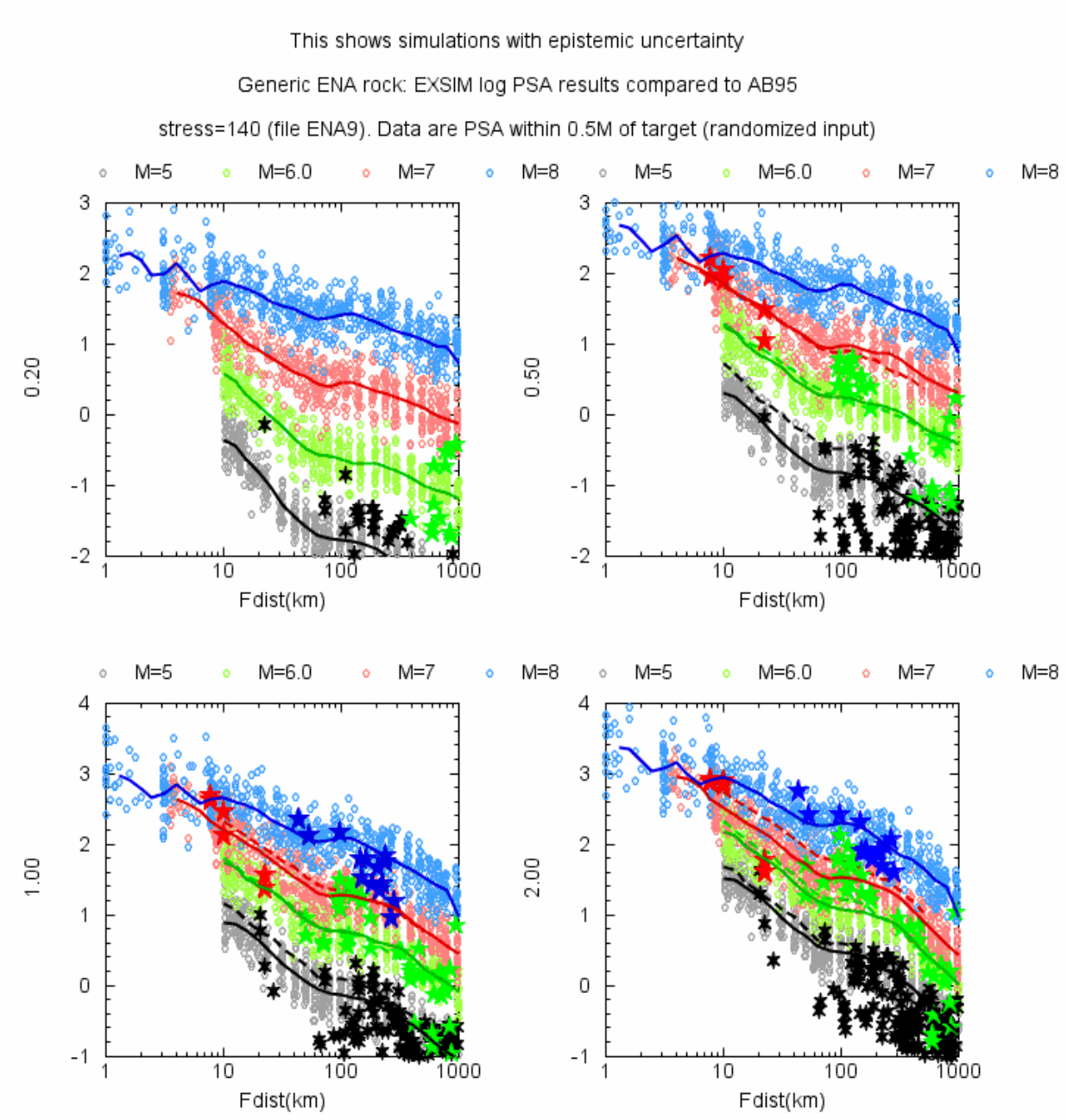

Figure 3a – Log values of horizontal component 5% pseudo-acceleration at frequencies 0.2, 0.5, 1 and 2 Hz, for ENA rock sites, for **M** 5, 6, 7 and 8. Dots show PSA from simulations, including epistemic uncertainty. Stars show ENA data (Table 6) within 0.5 magnitude units of each plotted magnitude value (color-coded). Dashed lines show ENA ground-motion relations of Atkinson and Boore (1995). Solid lines show mean predicted amplitudes from simulations.

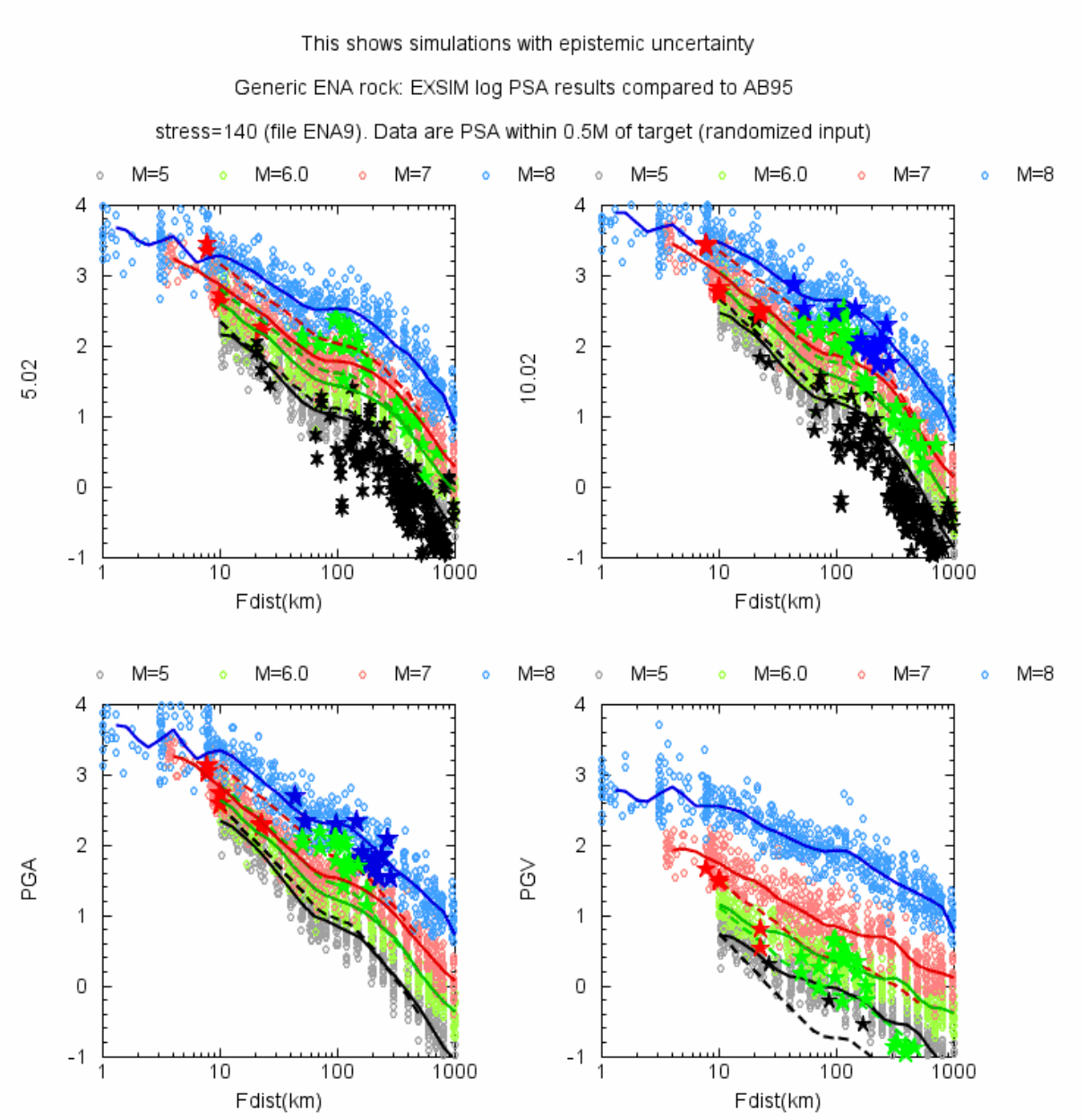

Figure 3b – Log horizontal component 5% pseudo-acceleration at frequencies of 5, 10 Hz, PGA, PGV, for ENA rock sites, for **M** 5, 6, 7 and 8. Dots show PSA from simulations, including epistemic uncertainty. Stars show ENA data (Table 6) within 0.5 magnitude units of each plotted magnitude value (color-coded). Dashed lines show ENA ground-motion relations of Atkinson and Boore (1995). Solid lines show mean predicted amplitudes from simulations.

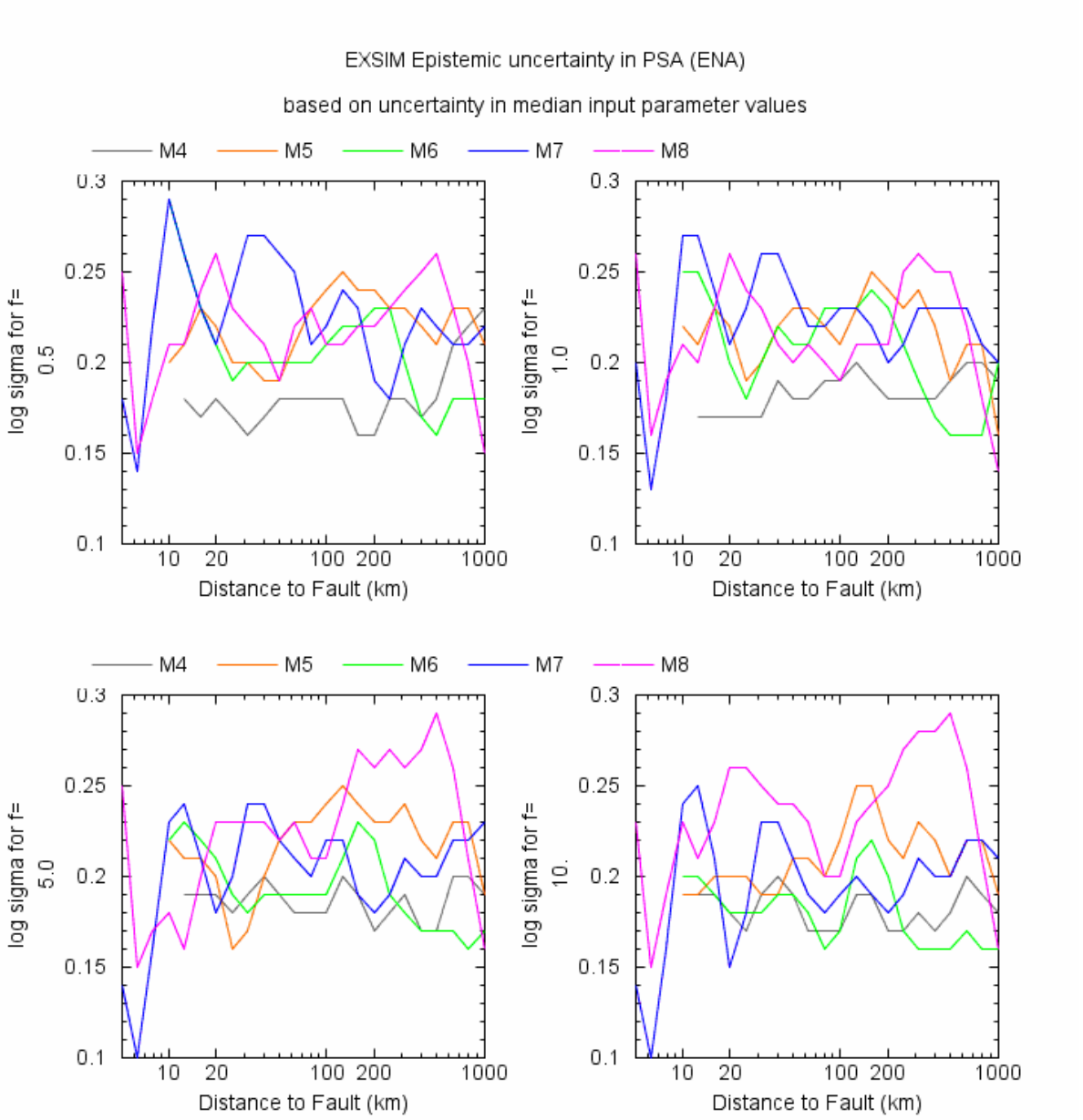
EXSIM Epistemic uncertainty in PSA (ENA)
based on uncertainty in median input parameter values
M4
M5
M6
M7
M8
log sigma for f= 0.5
log sigma for f= 1.0
log sigma for f= 5.0
log sigma for f= 10.
0.3
0.25
0.2
0.15
0.1
10
20
100
200
1000
Distance to Fault (km)

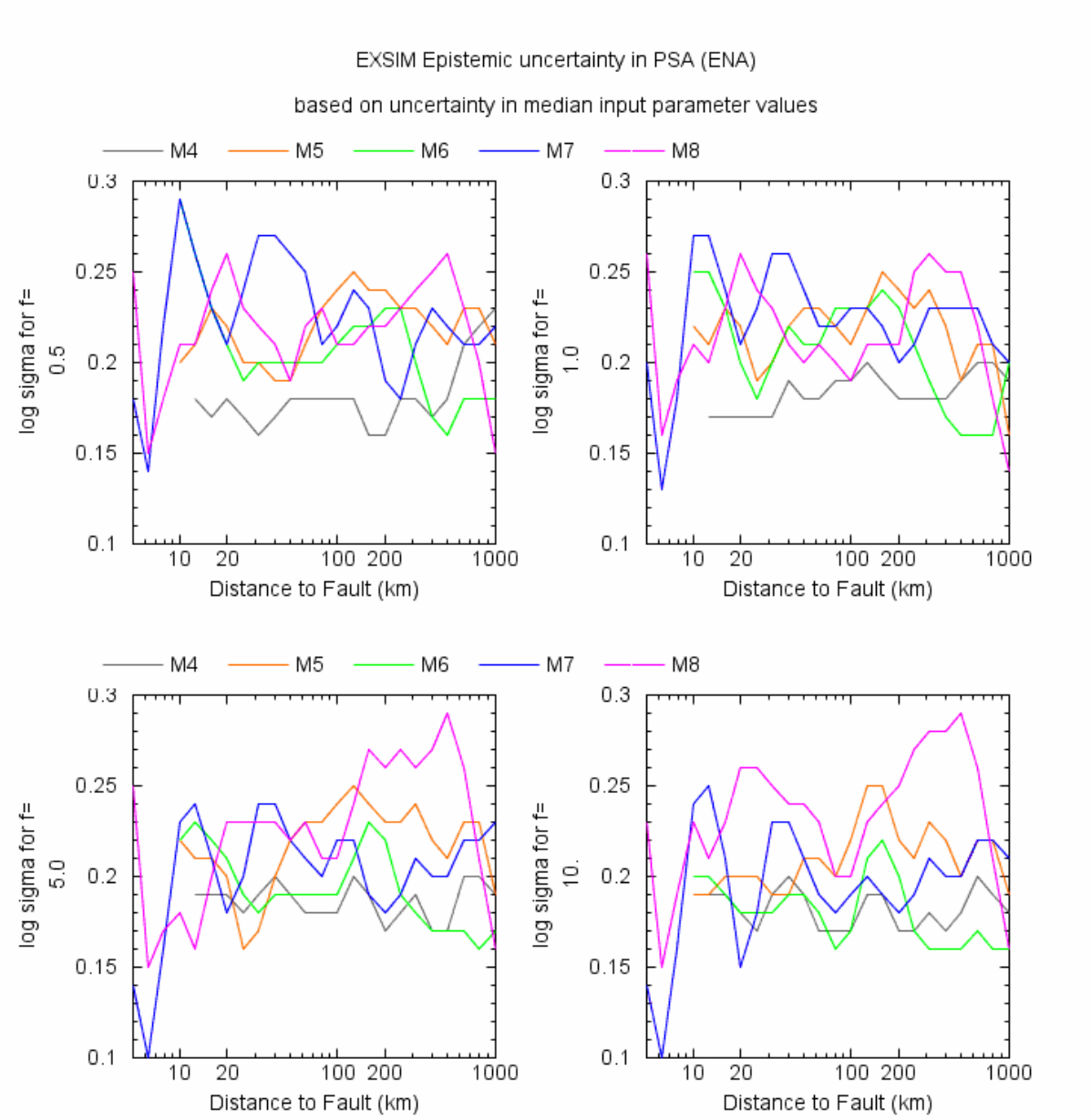

Figure 4 – Epistemic uncertainty in median ENA ground motion relations based on uncertainty in median model parameters.

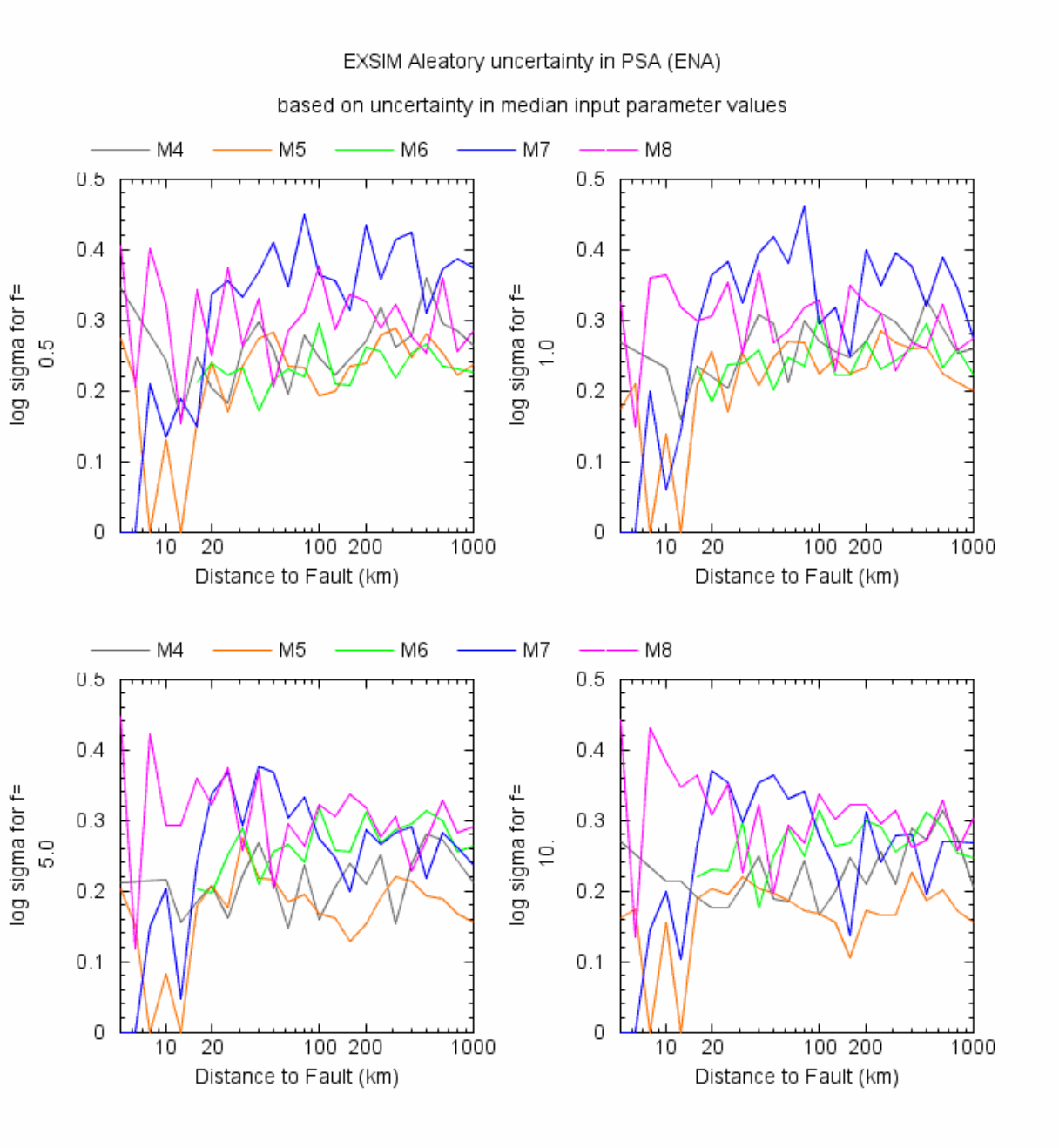

Figure 5 – Aleatory uncertainty (variability) in ENA ground motions based on variability of model parameters

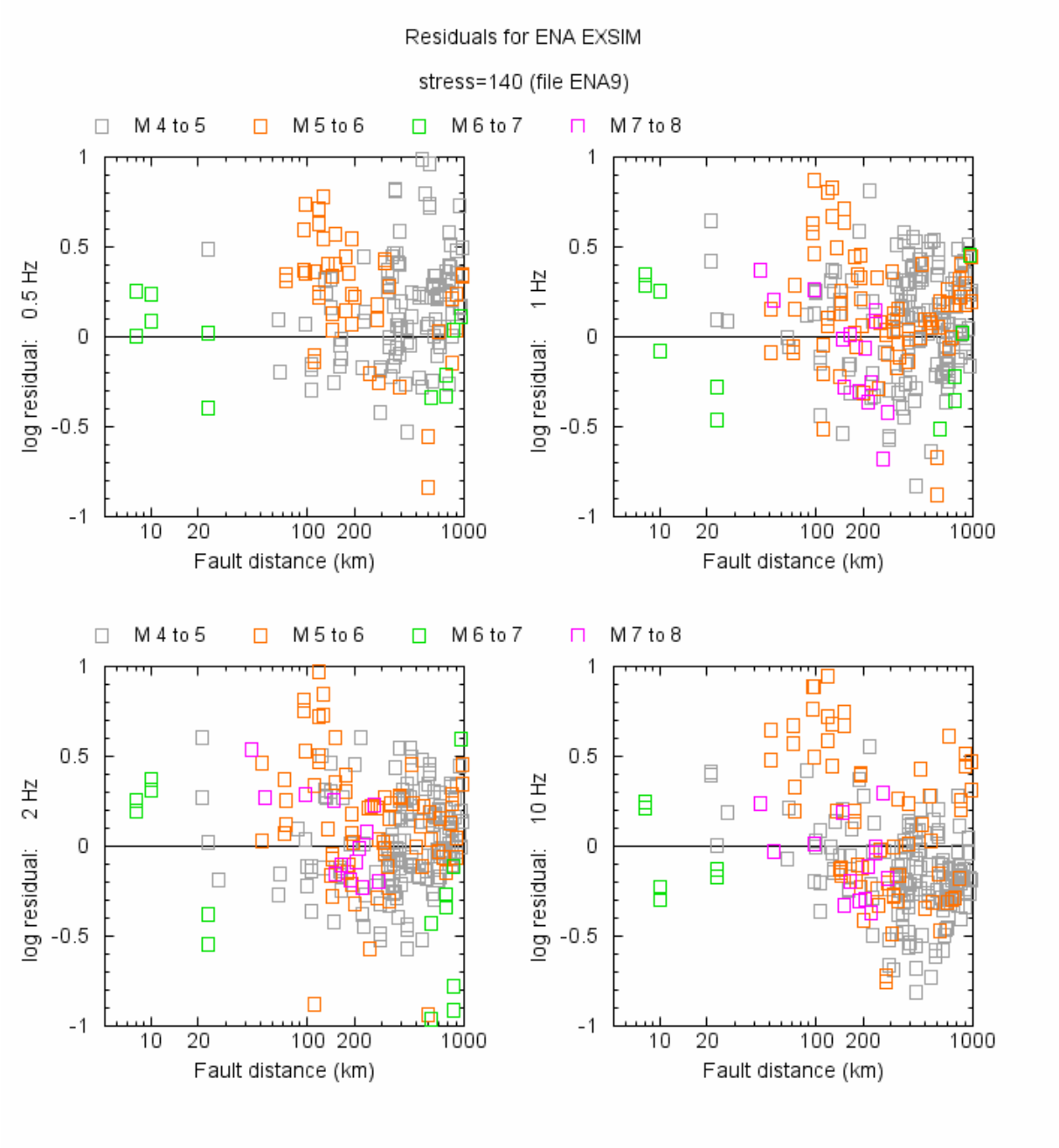

Figure 6 – Residuals of ENA ground-motion relations (Table 5) based on comparison with ground-motion data (Table 6).

Table 1 – Median Parameter values for ENA ground-motion simulations with EXSIM

Parameter	**Median Value**
Shear-wave velocity (at 13 km depth) (β)	3.7 km/s
Density (mid-crustal)	2.8 gm/cm^3
Rupture propagation speed	0.8 β
Stress drop	140 bars
Pulsing Percentage	25%
Kappa	0.004
Geometric spreading, R^b: b =	-1.3 (0 to 70 km) +0.2 (70 to 140 km) -0.5 (>140 km)
Distance dependence of duration, *d* R, *d* =	+0.16 (0 to 70 km) -0.03 (70 to 130 km) +0.04 (>130 km)
Quality factor	$Q = 893\ f^{0.32}$ ($Q_{minimum}$ = 1000)
Fault dip	50˚
Slip distribution and hypocenter location	Random

Table 2 – Epistemic Uncertainty in Key Model Parameters

Parameter	Distribution type	Median	Standard Deviation	Minimum	Maximum
Fault Dip	Normal	50.	10.	30.	70.
Log stress	Normal	2.14	0.054		
Pulsing%	Random			10.	50.
Kappa	Random			0.002	0.006
b1 (R<70)	Normal	-1.3	0.1		
b2 (70-140)	Normal	+0.2	0.2		
Depth	Normal	13.	3.		
Fault length factor	Random			0.3	0.7
Fault width factor	Random			0.6	0.8

Table 3 – Aleatory Uncertainty (variability) in Key Model Parameters

Parameter	Distribution type	Median	Standard Deviation	Minimum	Maximum
Fault Dip	Normal	50.	20.	10.	90.
Log stress	Normal	2.14	0.31		
Pulsing%	Random			10.	90.
Kappa	Random			0.002	0.01
b1 (R<70)	Random	-1.3		-1.5	-1.1
b2 (70-140)	Random	+0.2		-0.5	+0.9
Depth	Normal	13.	10.	2.	30.
Fault length factor	Random			0.2	0.8
Fault width factor	Random			0.4	1.0

Table 4 – Stress drops for ENA events of **M**≥4 based on high-frequency spectral level at 20 km (Ahf). Reference MMI indicates Ahf inferred from intensity data, AC97 indicates Ahf based on spectral data of Atkinson and Chen (1997), A1993 indicates Ahf from spectral data of Atkinson (1993), A2004 indicates Ahf from spectral data of Atkinson (2004). Ahf is in log cgs units.

Event Information				Observed	Inferred		
year	mo	dy	Moment M	Ahf (20km)	Ahf(MMI)	Reference	Stress(bars)
1811			7.5		1.66	MMI	338
1886			7.0		1.38	MMI	202
1925	3	1	6.4	1.20		AC97	214
1929	8	12	4.9		0.34	MMI	134
1929	11	18	7.3	1.90		AC97	909
1935	11	1	6.2	0.60		AC97	35
1939	10	19	5.3		0.51	MMI	112
1940	12	20	5.5		0.55	MMI	89
1944	9	5	5.8	0.60		AC97	64
1968	11	9	5.4		0.90	MMI	354
1980	8	27	5.1		0.57	MMI	198
1982	1	9	4.6		-0.05	MMI	67
1982	1	9	5.5		0.47	MMI	69
1982	1	11	5.2	0.37		A2004	84
1982	1	19	4.3	-0.13		A2004	100
1982	3	31	4.2	-0.15		A2004	119
1982	6	16	4.2	-0.23		A2004	91
1983	10	7	5.0	0.51		A2004	198
1985	10	5	6.7	1.22		A1993	158
1985	12	23	6.8	1.12		A1993	100
1985	12	25	5.2	0.22		A1993	50
1986	1	31	4.8	0.32		A2004	156
1986	7	12	4.5	0.15		A2004	167
1987	6	10	5.0	0.55		A1993	229
1988	3	25	6.3	0.92		A1993	93
1988	11	23	4.3	-0.18		A2004	84
1988	11	25	5.8	1.28		A1993	673
1989	3	16	5.0	0.47		A1993	174
1989	12	25	5.9	0.97		A1993	197
1990	10	19	4.7	0.33		A2004	198
1997	11	6	4.5	-0.14		A2004	60
1998	9	25	4.5	0.40		A2004	393
1999	3	16	4.5	0.04		A2004	116
2000	1	1	4.7	0.22		A2004	138
2002	4	20	5.0	0.07		A2004	44

Table 5 – Predicted Median ENA ground motions on hard rock (horizontal component, log(10) values are given in cgs units) for 5% damped PSA at stated frequencies.

Magnitude	Dfault	0.2	0.5	1	2	5	10	PGA	PGV
3.5	13	-2.37	-1.61	-1.02	-0.32	0.61	1.23	1.32	-0.48
3.5	16	-2.51	-1.74	-1.13	-0.44	0.53	1.13	1.22	-0.44
3.5	20	-2.70	-1.93	-1.29	-0.58	0.39	0.98	1.06	-0.48
3.5	25	-2.90	-2.11	-1.47	-0.73	0.22	0.79	0.85	-0.61
3.5	32	-3.14	-2.33	-1.67	-0.94	0.02	0.57	0.60	-0.80
3.5	40	-3.37	-2.56	-1.89	-1.16	-0.18	0.36	0.36	-0.92
3.5	50	-3.56	-2.75	-2.08	-1.34	-0.38	0.17	0.11	-0.96
3.5	63	-3.70	-2.88	-2.22	-1.47	-0.53	0.03	-0.08	-1.03
3.5	79	-3.75	-2.93	-2.26	-1.52	-0.56	-0.04	-0.18	-1.10
3.5	100	-3.78	-2.96	-2.29	-1.54	-0.58	-0.08	-0.26	-1.17
3.5	126	-3.84	-3.01	-2.34	-1.59	-0.64	-0.15	-0.38	-1.28
3.5	159	-3.92	-3.10	-2.42	-1.66	-0.74	-0.27	-0.55	-1.42
3.5	200	-4.02	-3.18	-2.49	-1.74	-0.84	-0.40	-0.74	-1.56
3.5	251	-4.12	-3.27	-2.57	-1.82	-0.93	-0.53	-0.92	-1.70
3.5	316	-4.26	-3.41	-2.70	-1.95	-1.08	-0.74	-1.17	-1.83
3.5	398	-4.44	-3.60	-2.88	-2.11	-1.30	-1.02	-1.48	-1.96
3.5	501	-4.62	-3.77	-3.05	-2.30	-1.54	-1.33	-1.82	-2.17
3.5	631	-4.78	-3.92	-3.22	-2.48	-1.79	-1.67	-2.16	-2.47
3.5	794	-4.96	-4.07	-3.37	-2.69	-2.06	-2.06	-2.51	-2.71
3.5	1000	-5.11	-4.21	-3.51	-2.88	-2.30	-2.39	-2.80	-2.84
4.0	13	-1.63	-0.88	-0.27	0.42	1.33	1.79	1.73	-0.05
4.0	16	-1.83	-1.08	-0.45	0.26	1.17	1.61	1.54	-0.11
4.0	20	-2.08	-1.30	-0.64	0.08	0.99	1.43	1.32	-0.19
4.0	25	-2.31	-1.50	-0.81	-0.10	0.81	1.25	1.12	-0.32
4.0	32	-2.52	-1.70	-0.99	-0.27	0.63	1.06	0.90	-0.48
4.0	40	-2.74	-1.91	-1.20	-0.45	0.41	0.84	0.65	-0.60
4.0	50	-2.90	-2.06	-1.36	-0.59	0.24	0.67	0.45	-0.60
4.0	63	-3.00	-2.15	-1.45	-0.67	0.16	0.57	0.33	-0.62
4.0	79	-3.05	-2.20	-1.51	-0.72	0.12	0.50	0.23	-0.69
4.0	100	-3.06	-2.22	-1.53	-0.75	0.11	0.47	0.18	-0.73
4.0	126	-3.08	-2.24	-1.54	-0.77	0.09	0.43	0.11	-0.78
4.0	159	-3.16	-2.30	-1.58	-0.84	-0.02	0.32	-0.05	-0.91
4.0	200	-3.25	-2.38	-1.65	-0.92	-0.14	0.18	-0.23	-1.04
4.0	251	-3.34	-2.47	-1.73	-0.99	-0.23	0.06	-0.39	-1.16
4.0	316	-3.49	-2.61	-1.87	-1.12	-0.38	-0.16	-0.62	-1.29
4.0	398	-3.68	-2.80	-2.03	-1.31	-0.62	-0.46	-0.94	-1.40
4.0	501	-3.82	-2.93	-2.16	-1.47	-0.85	-0.75	-1.23	-1.57
4.0	631	-3.94	-3.03	-2.29	-1.60	-1.06	-1.04	-1.50	-1.81
4.0	794	-4.08	-3.17	-2.43	-1.78	-1.31	-1.40	-1.80	-2.01
4.0	1000	-4.22	-3.31	-2.57	-1.97	-1.54	-1.71	-2.05	-2.09
4.5	13	-1.07	-0.36	0.27	0.96	1.76	2.09	2.00	0.38

4.5	16	-1.29	-0.55	0.11	0.81	1.57	1.92	1.79	0.24
4.5	20	-1.47	-0.69	-0.01	0.69	1.44	1.79	1.64	0.15
4.5	25	-1.63	-0.83	-0.12	0.59	1.33	1.65	1.48	0.04
4.5	32	-1.87	-1.03	-0.31	0.41	1.13	1.45	1.25	-0.14
4.5	40	-2.08	-1.21	-0.48	0.24	0.94	1.24	1.02	-0.25
4.5	50	-2.24	-1.35	-0.62	0.10	0.77	1.05	0.81	-0.25
4.5	63	-2.39	-1.50	-0.76	-0.06	0.63	0.90	0.62	-0.32
4.5	79	-2.47	-1.59	-0.83	-0.15	0.56	0.82	0.52	-0.40
4.5	100	-2.49	-1.60	-0.85	-0.16	0.53	0.81	0.47	-0.44
4.5	126	-2.53	-1.63	-0.88	-0.20	0.50	0.75	0.37	-0.51
4.5	159	-2.61	-1.70	-0.95	-0.27	0.41	0.62	0.23	-0.62
4.5	200	-2.67	-1.75	-1.00	-0.32	0.31	0.49	0.07	-0.73
4.5	251	-2.73	-1.80	-1.03	-0.38	0.20	0.35	-0.08	-0.85
4.5	316	-2.84	-1.91	-1.13	-0.49	0.05	0.16	-0.29	-0.94
4.5	398	-3.00	-2.07	-1.31	-0.66	-0.15	-0.10	-0.55	-1.01
4.5	501	-3.16	-2.20	-1.47	-0.85	-0.38	-0.40	-0.83	-1.18
4.5	631	-3.27	-2.30	-1.57	-1.00	-0.61	-0.71	-1.09	-1.40
4.5	794	-3.39	-2.42	-1.69	-1.17	-0.87	-1.05	-1.37	-1.57
4.5	1000	-3.53	-2.56	-1.82	-1.35	-1.12	-1.36	-1.62	-1.65
5.0	10	-0.36	0.30	0.89	1.52	2.16	2.47	2.35	0.72
5.0	13	-0.45	0.24	0.87	1.49	2.13	2.41	2.27	0.70
5.0	16	-0.63	0.11	0.78	1.39	2.02	2.28	2.13	0.61
5.0	20	-0.83	-0.05	0.64	1.27	1.88	2.15	1.97	0.49
5.0	25	-1.03	-0.23	0.48	1.12	1.75	1.99	1.79	0.35
5.0	32	-1.27	-0.41	0.31	0.94	1.56	1.79	1.58	0.21
5.0	40	-1.45	-0.56	0.17	0.81	1.36	1.60	1.36	0.14
5.0	50	-1.59	-0.68	0.05	0.69	1.20	1.42	1.16	0.12
5.0	63	-1.71	-0.79	-0.06	0.55	1.09	1.29	1.00	0.06
5.0	79	-1.75	-0.82	-0.11	0.50	1.03	1.23	0.92	0.00
5.0	100	-1.77	-0.83	-0.14	0.48	0.99	1.19	0.85	-0.04
5.0	126	-1.81	-0.87	-0.17	0.45	0.95	1.14	0.77	-0.11
5.0	159	-1.84	-0.89	-0.19	0.41	0.90	1.06	0.67	-0.18
5.0	200	-1.91	-0.94	-0.27	0.31	0.78	0.90	0.49	-0.31
5.0	251	-2.01	-1.03	-0.36	0.20	0.65	0.72	0.31	-0.46
5.0	316	-2.11	-1.13	-0.47	0.09	0.49	0.52	0.11	-0.54
5.0	398	-2.20	-1.21	-0.56	-0.04	0.32	0.28	-0.09	-0.56
5.0	501	-2.30	-1.30	-0.67	-0.18	0.12	0.01	-0.32	-0.68
5.0	631	-2.42	-1.43	-0.82	-0.35	-0.13	-0.30	-0.59	-0.91
5.0	794	-2.51	-1.55	-0.95	-0.52	-0.40	-0.62	-0.86	-1.06
5.0	1000	-2.58	-1.63	-1.03	-0.67	-0.59	-0.86	-1.04	-1.08
5.5	13	0.09	0.81	1.39	1.90	2.41	2.63	2.46	0.98
5.5	16	-0.12	0.63	1.24	1.76	2.27	2.48	2.31	0.84
5.5	20	-0.32	0.47	1.11	1.63	2.12	2.33	2.15	0.70
5.5	25	-0.50	0.33	1.00	1.51	1.97	2.18	1.98	0.57
5.5	32	-0.68	0.21	0.86	1.38	1.82	2.03	1.79	0.49
5.5	40	-0.80	0.12	0.76	1.26	1.71	1.91	1.64	0.50

5.5	50	-0.94	0.00	0.64	1.16	1.59	1.76	1.48	0.48
5.5	63	-1.05	-0.12	0.52	1.03	1.45	1.61	1.30	0.38
5.5	79	-1.11	-0.20	0.45	0.93	1.36	1.52	1.18	0.28
5.5	100	-1.16	-0.24	0.41	0.89	1.29	1.43	1.09	0.20
5.5	126	-1.21	-0.30	0.37	0.85	1.23	1.35	1.00	0.13
5.5	159	-1.26	-0.35	0.31	0.80	1.16	1.26	0.88	0.05
5.5	200	-1.30	-0.38	0.25	0.72	1.05	1.15	0.74	-0.05
5.5	251	-1.38	-0.44	0.18	0.62	0.94	1.00	0.59	-0.16
5.5	316	-1.49	-0.55	0.06	0.49	0.77	0.79	0.39	-0.24
5.5	398	-1.59	-0.66	-0.06	0.34	0.58	0.55	0.18	-0.28
5.5	501	-1.66	-0.74	-0.15	0.20	0.39	0.29	-0.03	-0.38
5.5	631	-1.73	-0.82	-0.27	0.05	0.16	0.01	-0.25	-0.57
5.5	794	-1.83	-0.92	-0.40	-0.13	-0.10	-0.30	-0.50	-0.71
5.5	1000	-1.92	-1.00	-0.48	-0.27	-0.28	-0.53	-0.67	-0.71
6.0	10	0.58	1.24	1.75	2.18	2.60	2.80	2.63	1.15
6.0	13	0.46	1.15	1.67	2.11	2.50	2.71	2.54	1.08
6.0	16	0.28	0.99	1.52	1.97	2.34	2.55	2.36	0.94
6.0	20	0.11	0.85	1.41	1.84	2.22	2.42	2.20	0.83
6.0	25	-0.02	0.76	1.34	1.75	2.13	2.32	2.09	0.79
6.0	32	-0.17	0.65	1.22	1.62	1.98	2.18	1.94	0.77
6.0	40	-0.34	0.50	1.05	1.45	1.81	1.99	1.75	0.70
6.0	50	-0.48	0.38	0.92	1.31	1.65	1.82	1.55	0.58
6.0	63	-0.57	0.28	0.82	1.20	1.53	1.69	1.39	0.46
6.0	79	-0.59	0.24	0.78	1.12	1.47	1.61	1.29	0.39
6.0	100	-0.63	0.24	0.77	1.08	1.43	1.56	1.23	0.35
6.0	126	-0.69	0.21	0.74	1.06	1.39	1.50	1.16	0.30
6.0	159	-0.70	0.16	0.69	1.04	1.33	1.43	1.07	0.23
6.0	200	-0.70	0.13	0.62	0.98	1.24	1.30	0.94	0.14
6.0	251	-0.75	0.09	0.58	0.92	1.13	1.16	0.80	0.10
6.0	316	-0.82	0.04	0.53	0.83	1.00	1.00	0.65	0.11
6.0	398	-0.91	-0.07	0.40	0.66	0.80	0.74	0.42	0.02
6.0	501	-1.01	-0.19	0.25	0.46	0.56	0.45	0.17	-0.18
6.0	631	-1.07	-0.28	0.14	0.32	0.34	0.19	-0.03	-0.30
6.0	794	-1.12	-0.35	0.03	0.18	0.12	-0.07	-0.21	-0.33
6.0	1000	-1.19	-0.42	-0.10	0.02	-0.08	-0.28	-0.37	-0.38
6.5	5	1.60	2.22	2.61	2.94	3.32	3.56	3.43	2.05
6.5	6	1.57	2.15	2.52	2.88	3.22	3.45	3.32	1.99
6.5	8	1.34	1.93	2.34	2.67	3.03	3.23	3.10	1.82
6.5	10	1.12	1.76	2.22	2.53	2.89	3.08	2.94	1.68
6.5	13	0.97	1.67	2.12	2.45	2.79	2.96	2.81	1.59
6.5	16	0.84	1.56	1.97	2.34	2.66	2.85	2.68	1.49
6.5	20	0.75	1.46	1.87	2.25	2.57	2.77	2.57	1.43
6.5	25	0.64	1.37	1.79	2.14	2.48	2.65	2.42	1.37
6.5	32	0.51	1.28	1.68	2.01	2.33	2.49	2.25	1.26
6.5	40	0.39	1.15	1.56	1.88	2.18	2.34	2.08	1.13
6.5	50	0.28	1.02	1.43	1.76	2.03	2.19	1.92	1.01

6.5	63	0.22	0.94	1.36	1.67	1.95	2.09	1.81	0.95
6.5	79	0.22	0.93	1.36	1.64	1.93	2.04	1.75	0.94
6.5	100	0.24	0.95	1.36	1.64	1.93	2.04	1.71	0.90
6.5	126	0.26	1.00	1.38	1.66	1.94	2.03	1.69	0.86
6.5	159	0.20	0.98	1.36	1.60	1.87	1.91	1.57	0.81
6.5	200	0.10	0.88	1.27	1.48	1.72	1.73	1.39	0.74
6.5	251	0.08	0.83	1.20	1.41	1.60	1.61	1.26	0.71
6.5	316	0.06	0.78	1.12	1.34	1.47	1.45	1.12	0.67
6.5	398	-0.03	0.67	0.99	1.18	1.26	1.21	0.91	0.53
6.5	501	-0.12	0.56	0.86	1.01	1.04	0.94	0.70	0.35
6.5	631	-0.19	0.46	0.74	0.85	0.82	0.68	0.50	0.25
6.5	794	-0.27	0.34	0.61	0.68	0.58	0.40	0.29	0.21
6.5	1000	-0.33	0.24	0.51	0.53	0.38	0.20	0.14	0.16
7.0	4	1.71	2.21	2.63	2.94	3.24	3.45	3.27	1.93
7.0	5	1.68	2.14	2.57	2.92	3.16	3.36	3.21	1.94
7.0	6	1.59	2.06	2.47	2.82	3.07	3.25	3.12	1.91
7.0	8	1.44	1.96	2.32	2.64	2.97	3.15	2.98	1.83
7.0	10	1.28	1.85	2.19	2.51	2.86	3.03	2.82	1.74
7.0	13	1.15	1.73	2.11	2.41	2.74	2.90	2.68	1.63
7.0	16	1.02	1.64	2.01	2.31	2.63	2.77	2.54	1.55
7.0	20	0.91	1.55	1.91	2.20	2.52	2.65	2.40	1.49
7.0	25	0.80	1.43	1.79	2.09	2.40	2.53	2.25	1.38
7.0	32	0.69	1.29	1.65	1.94	2.25	2.38	2.08	1.24
7.0	40	0.60	1.19	1.54	1.81	2.10	2.23	1.93	1.16
7.0	50	0.53	1.10	1.43	1.71	1.97	2.10	1.79	1.08
7.0	63	0.43	0.97	1.30	1.58	1.85	1.96	1.64	0.96
7.0	79	0.39	0.93	1.26	1.52	1.78	1.88	1.56	0.86
7.0	100	0.44	0.98	1.28	1.54	1.79	1.87	1.53	0.84
7.0	126	0.44	0.97	1.27	1.52	1.77	1.82	1.47	0.79
7.0	159	0.38	0.90	1.22	1.46	1.70	1.73	1.38	0.71
7.0	200	0.33	0.87	1.18	1.41	1.62	1.64	1.28	0.70
7.0	251	0.28	0.87	1.14	1.35	1.50	1.51	1.16	0.70
7.0	316	0.21	0.79	1.05	1.24	1.35	1.33	1.00	0.61
7.0	398	0.15	0.65	0.91	1.08	1.15	1.07	0.79	0.43
7.0	501	0.09	0.54	0.79	0.91	0.94	0.81	0.59	0.28
7.0	631	0.00	0.45	0.68	0.75	0.72	0.56	0.41	0.22
7.0	794	-0.08	0.36	0.55	0.57	0.47	0.31	0.22	0.18
7.0	1000	-0.13	0.31	0.44	0.43	0.28	0.14	0.08	0.11
7.5	4	1.83	2.30	2.65	2.95	3.34	3.55	3.42	2.30
7.5	5	1.75	2.24	2.57	2.92	3.29	3.53	3.39	2.27
7.5	6	1.67	2.18	2.52	2.88	3.26	3.49	3.37	2.25
7.5	8	1.69	2.20	2.54	2.86	3.25	3.45	3.33	2.28
7.5	10	1.65	2.14	2.48	2.77	3.15	3.34	3.20	2.25
7.5	13	1.59	2.06	2.40	2.68	3.05	3.23	3.08	2.20
7.5	16	1.54	2.02	2.36	2.61	2.97	3.13	2.96	2.10
7.5	20	1.45	1.96	2.25	2.51	2.85	3.03	2.81	1.95

7.5	25	1.35	1.87	2.13	2.42	2.76	2.92	2.69	1.88
7.5	32	1.24	1.74	2.03	2.32	2.63	2.76	2.53	1.80
7.5	40	1.11	1.60	1.91	2.17	2.45	2.58	2.32	1.68
7.5	50	1.02	1.51	1.81	2.05	2.32	2.47	2.18	1.59
7.5	63	1.00	1.48	1.77	2.01	2.27	2.41	2.11	1.56
7.5	79	1.03	1.49	1.77	2.02	2.27	2.39	2.07	1.54
7.5	100	1.06	1.50	1.78	2.01	2.25	2.36	2.02	1.49
7.5	126	1.02	1.44	1.72	1.97	2.18	2.29	1.93	1.42
7.5	159	0.96	1.37	1.64	1.92	2.11	2.19	1.82	1.36
7.5	200	0.92	1.36	1.61	1.86	2.05	2.08	1.72	1.31
7.5	251	0.86	1.31	1.56	1.79	1.94	1.95	1.61	1.22
7.5	316	0.80	1.22	1.47	1.70	1.80	1.79	1.46	1.10
7.5	398	0.77	1.15	1.38	1.57	1.64	1.59	1.29	0.98
7.5	501	0.73	1.08	1.30	1.43	1.48	1.36	1.12	0.91
7.5	631	0.65	0.99	1.18	1.26	1.26	1.11	0.94	0.85
7.5	794	0.57	0.90	1.05	1.09	1.02	0.86	0.76	0.76
7.5	1000	0.52	0.85	0.96	0.99	0.87	0.71	0.65	0.68
8.0	0	2.25	2.73	3.04	3.33	3.67	3.87	3.70	2.77
8.0	1	2.25	2.68	2.97	3.36	3.68	3.89	3.70	2.78
8.0	2	2.29	2.64	2.91	3.34	3.64	3.88	3.68	2.77
8.0	2	2.17	2.47	2.78	3.17	3.50	3.74	3.50	2.64
8.0	3	1.98	2.30	2.65	3.03	3.43	3.62	3.38	2.61
8.0	3	2.00	2.40	2.73	3.08	3.49	3.67	3.52	2.74
8.0	4	2.13	2.54	2.85	3.15	3.56	3.73	3.63	2.83
8.0	5	1.96	2.35	2.71	3.00	3.38	3.59	3.43	2.71
8.0	6	1.75	2.15	2.58	2.85	3.17	3.45	3.23	2.55
8.0	8	1.82	2.25	2.63	2.91	3.24	3.50	3.31	2.55
8.0	10	1.88	2.29	2.65	2.94	3.28	3.48	3.34	2.56
8.0	13	1.83	2.22	2.60	2.88	3.21	3.39	3.26	2.51
8.0	16	1.78	2.20	2.55	2.81	3.14	3.31	3.14	2.46
8.0	20	1.69	2.14	2.46	2.71	3.03	3.22	3.00	2.35
8.0	25	1.59	2.03	2.35	2.60	2.91	3.10	2.85	2.25
8.0	32	1.54	1.96	2.26	2.51	2.80	2.97	2.71	2.17
8.0	40	1.49	1.88	2.18	2.41	2.69	2.85	2.56	2.10
8.0	50	1.41	1.78	2.08	2.31	2.58	2.73	2.43	2.02
8.0	63	1.35	1.74	2.04	2.27	2.52	2.65	2.34	1.94
8.0	79	1.36	1.77	2.05	2.27	2.51	2.64	2.31	1.90
8.0	100	1.41	1.84	2.09	2.30	2.54	2.65	2.31	1.92
8.0	126	1.43	1.82	2.08	2.29	2.52	2.61	2.26	1.91
8.0	159	1.37	1.73	2.00	2.21	2.43	2.48	2.12	1.80
8.0	200	1.31	1.66	1.91	2.10	2.31	2.34	1.97	1.68
8.0	251	1.23	1.58	1.81	1.97	2.15	2.15	1.80	1.58
8.0	316	1.15	1.49	1.71	1.85	2.00	1.95	1.63	1.47
8.0	398	1.11	1.45	1.64	1.79	1.89	1.79	1.52	1.39
8.0	501	1.05	1.38	1.54	1.66	1.70	1.58	1.36	1.31
8.0	631	0.98	1.27	1.42	1.50	1.48	1.34	1.19	1.22
8.0	794	0.95	1.20	1.34	1.38	1.31	1.15	1.06	1.12
8.0	1000	0.71	0.87	0.97	0.96	0.89	0.78	0.73	0.77

Table 6 – ENA response spectra database for rock sites in log cgs units. Vertical-component data (Z) converted to equivalent horizontal where required using H/V ratios shown.

H/V used to convert vertical			1	1	1.13	1.22	1.36	1.41				
Event	M	R(km)	0.2 Hz	0.5 Hz	1 Hz	2 Hz	5 Hz	10 Hz	PGA	PGV	stn	comp
01/03/1925	6.4	960	-0.43	0.23	0.85	1.04						
01/03/1925	6.4	862	-1.68	-1.10	-0.60	-0.26						
18/11/1929	7.3	1459	-0.62	-0.36	0.11							
18/11/1929	7.3	2199	-1.07	-0.55	-0.02							
18/11/1929	7.3	2199	-0.74	-0.26	0.20							
01/11/1935	6.2	616	-0.74	-0.32	-0.13	0.11						
01/11/1935	6.2	616	-1.28	-1.11	-0.77	-0.42						
01/11/1935	6.2	428	-2.01	-1.20	-0.55							
01/11/1935	6.2	869	-1.74	-1.28	-0.96	-0.60						
01/11/1935	6.2	1430	-2.18	-1.68	-1.55	-1.24						
01/11/1935	6.2	861	-0.54	-0.07	0.23	0.20						
01/11/1935	6.2	783	-0.74	-0.41	0.04	0.04						
01/11/1935	6.2	783	-0.52	-0.29	-0.10	0.11						
05/09/1944	5.8	389	-1.49	-0.59	0.08							
05/09/1944	5.8	1007	-1.46	-0.89	-0.36							
05/09/1944	5.8	698	-1.47	-0.51	0.18							
05/09/1944	5.8	599	-1.70	-1.04	-0.68	-0.70						
05/09/1944	5.8	599	-1.59	-1.32	-0.89	-0.80						
19/01/1982	4.3	275			-1.46	-0.82	-0.17	0.11		-2.17	MNT	Z
19/01/1982	4.3	324			-1.36	-1.00	-0.57	-0.49		-2.59	GNT	Z
19/01/1982	4.3	389			-1.62	-0.66	-0.22	-0.11		-2.33	OTT	Z
19/01/1982	4.3	537			-1.74	-1.01	-0.68	-0.74		-2.71	CKO	Z
19/01/1982	4.3	724			-1.96	-1.38	-1.17	-1.38		-2.85	VDQ	Z
19/01/1982	4.3	1175			-2.15	-2.00	-2.02	-2.24		-3.39	JAQ	Z
07/10/1983	5.0	143			-0.41	0.26	0.70	0.96		-1.20	WBO	Z
07/10/1983	5.0	180			-0.29	0.20	0.86	0.77		-1.47	MNT	Z
07/10/1983	5.0	199			-0.21	0.32	0.54	0.78		-1.48	OTT	Z
07/10/1983	5.0	246			-0.03	0.41	0.60	0.49		-1.11	SBQ	Z
07/10/1983	5.0	257			-0.30	0.40	0.88	0.67		-1.22	TRQ	Z
07/10/1983	5.0	309			-0.10	0.11	0.15	0.04		-1.45	GNT	Z
07/10/1983	5.0	324			-0.66	-0.05	0.45	0.32		-1.66	GRQ	Z
07/10/1983	5.0	339			-0.62	0.28	0.18	0.28		-1.46	CKO	Z
07/10/1983	5.0	501			-0.59	-0.19	-0.03	-0.35		-1.82	LPQ	Z
07/10/1983	5.0	562			-0.70	-0.06	-0.11	-0.47		-1.87	VDQ	Z
07/10/1983	5.0	603			-0.74	-0.14	-0.21	-0.40		-1.75	GGN	Z
07/10/1983	5.0	617			-0.62	-0.30	-0.54	-0.74		-2.10	EBN	Z
07/10/1983	5.0	692			-0.70	-0.46	-0.57	-0.74		-1.92	KLN	Z
07/10/1983	5.0	741			-0.92	-0.54	-0.49	-0.82		-2.16	HTQ	Z
07/10/1983	5.0	776			-0.77	-0.66	-0.72	-0.89		-2.06	GSQ	Z
07/10/1983	5.0	832			-0.66	-0.43	-0.72	-0.85		-2.17	MNQ	Z
11/10/1983	3.6	24			-0.82	-0.07	0.72	0.92				Z
11/10/1983	3.6	159			-1.77	-0.92	-0.42	0.04				Z
11/10/1983	3.6	159			-1.82	-1.07	-0.42	-0.15				Z
11/10/1983	3.6	170			-1.80	-1.11	-0.43	-0.19				Z
11/10/1983	3.6	501			-2.07	-1.55	-1.49	-1.40				Z

11/10/1983	3.6	851		-3.17	-2.19	-1.72	1.82				Z
23/12/1985	6.8	8	1.95	2.62	2.86	3.45	3.40	3.03	1.66	S01	L
23/12/1985	6.8	8	2.20	2.68	2.91	3.34	3.43	3.12	1.65	S01	T
23/12/1985	6.8	10	2.04	2.45	2.88	2.72	2.75	2.58	1.52	S02	L
23/12/1985	6.8	10	1.89	2.11	2.83	2.61	2.81	2.73	1.48	S02	T
23/12/1985	6.8	23	1.04	1.36	1.60	2.20	2.49	2.28	0.53	S03	L
23/12/1985	6.8	23	1.46	1.54	1.76	2.26	2.45	2.26	0.80	S03	T
12/07/1986	4.5	794		-1.52	-1.02	-1.08	-1.28		-2.65	EEO	Z
12/07/1986	4.5	832		-1.47	-0.89	-0.96	-1.24		-2.67	CKO	Z
12/07/1986	4.5	884		-1.34	-1.00	-1.35	-1.33		-2.63	OTT	Z
12/07/1986	4.5	891		-1.52	-1.10	-1.28	-1.39		-2.81	WBO	Z
12/07/1986	4.5	959		-1.57	-1.12	-1.28	-1.49		-2.95	GRQ	Z
31/1/1986	4.8	21		0.76	1.28	1.89	2.38				H1
31/1/1986	4.8	21		0.99	1.61	2.04	2.36				H2
31/1/1986	4.8	525		-0.54	-0.27	-0.14	-0.43		-2.85	SUO	Z
31/1/1986	4.8	589		-0.74	-0.22	-0.12	-0.31		-1.88	EEO	Z
31/1/1986	4.8	603		-0.92	-0.44	-0.20	-0.36		-2.03	OTT	Z
31/1/1986	4.8	741		-0.92	-0.77	-0.77	-0.89		-2.35	MNT	Z
31/1/1986	4.8	776		-0.92	-0.57	-0.55			-2.08	VDQ	Z
31/1/1986	4.8	851		-0.89	-0.82	-0.85	-1.04		-2.29	SBQ	Z
31/1/1986	4.8	871		-0.96	-0.92	-0.85	-1.09		-2.31	GNT	Z
25/11/1988	5.8	51		0.70	1.26	2.00	2.26	2.02	0.18	S16	L
25/11/1988	5.8	51		0.94	1.69	2.15	2.41	2.10	0.40	S16	T
25/11/1988	5.8	71		0.61	1.45	2.08	2.18	2.18	0.26	S17	L
25/11/1988	5.8	71		0.58	1.15	2.00	2.28	1.95	-0.03	S17	T
25/11/1988	5.8	96	0.64	1.26	1.81	2.34	2.40	2.09	0.64	S20	L
25/11/1988	5.8	96	0.41	1.20	1.76	1.99	2.28	2.00	0.43	S20	T
25/11/1988	5.8	98	0.78	1.49	2.11	2.40	2.40	2.09	0.66	S08	L
25/11/1988	5.8	98	0.40	1.08	1.53	1.99	2.00	1.77	0.11	S08	T
25/11/1988	5.8	112	0.38	0.56	1.32	1.52		1.41	-0.24	S05	L
25/11/1988	5.8	118	0.23	0.65	1.70	2.28	2.52	2.08	0.43	S01	L
25/11/1988	5.8	118	0.26	0.70	1.48	2.23	2.40	1.98	0.38	S01	T
25/11/1988	5.8	118	0.72	1.40	1.45	1.97	2.04	1.60	0.34	S10	L
25/11/1988	5.8	118	0.64	1.40	1.94	1.97	2.18	1.75	0.54	S10	T
25/11/1988	5.8	126	0.78	1.41	1.70	1.99	1.88	1.65	0.41	S09	L
25/11/1988	5.8	126	0.54	1.26	1.81	2.26	2.11	1.74	0.41	S09	T
25/11/1988	5.8	151	0.53	1.18	1.30	1.96	2.11	1.70	0.18	S02	L
25/11/1988	5.8	151	0.36	1.26	1.54	2.11	2.04	1.70	0.34	S02	T
25/11/1988	5.8	178	0.08	0.52	1.30	1.76	1.49	1.15	-0.19	S14	L
25/11/1988	5.8	178	0.38	0.94	1.20	1.61	1.43	1.36	0.00	S14	T
25/11/1988	5.8	314		0.46	0.96	1.08	0.91		-0.86	GSQ	Z
25/11/1988	5.8	333		0.46	0.81	1.20	1.11		-0.81	TRQ	Z
25/11/1988	5.8	389		0.26	0.81	0.80	0.69		-0.97	KLN	Z
25/11/1988	5.8	391		0.20	0.82	0.99	0.91		-0.87	GRQ	Z
25/11/1988	5.8	468		0.11	0.85	0.92	0.89		-0.88	WBO	Z
25/11/1988	5.8	472		0.52	0.63	0.88	0.57		-0.88	GGN	Z
25/11/1988	5.8	537		0.15	0.41	0.60	0.58		-1.09	CKO	Z
25/11/1988	5.8	550		0.11	0.18	0.15	0.30		-1.09	LMN	Z
25/11/1988	5.8	708		-0.15	0.28	0.48	0.58		-1.47	JAQ	Z
19/10/1990	4.5	27		-0.10	0.34	1.43	1.77		0.33	GRQ	Z

19/10/1990	4.5	87			-0.72	-0.07	0.98	1.23	-0.19	TRQ	Z
19/10/1990	4.5	123			-0.57	0.30	0.60	0.74	-1.48	OTT	Z
19/10/1990	4.5	170			-0.66	-0.02	0.40	0.67	-0.54	WBO	Z
19/10/1990	4.5	191			-0.41	-0.30	0.45	0.88	-1.55	MNT	Z
19/10/1990	4.5	219			-0.21	0.26	0.79	0.98	-1.34	DPQ	Z
19/10/1990	4.5	407			-0.96	-0.38	0.20	-0.02	-1.82	A54	Z
19/10/1990	4.5	407			-1.21	-0.43	0.08	-0.05	-1.83	A11	Z
19/10/1990	4.5	417			-0.80	-0.68	-0.18	-0.43	-2.23	SWO	Z
19/10/1990	4.5	417			-0.96	-0.44	-0.17	-0.21	-2.38	SUO	Z
19/10/1990	4.5	437			-1.04	-0.40	-0.15	-0.38			Z
19/10/1990	4.5	437			-1.08	-0.57	-0.19	-0.30	-1.98	A16	Z
19/10/1990	4.5	437			-0.85	-0.47	0.00	-0.18	-2.25	A61	Z
19/10/1990	4.5	437			-1.26	-0.55	-0.16	-0.15			Z
19/10/1990	4.5	457			-1.11	-0.51	-0.18	-0.31	-2.30	SZO	Z
19/10/1990	4.5	457			-1.28	-0.64	-0.24	-0.27	-2.17	A64	Z
19/10/1990	4.5	468			-1.00	-0.30	0.26	-0.11	-2.06	A21	Z
23/11/1988	4.2	100			-1.01	-0.64	0.28	0.59	-1.62	A54	Z
23/11/1988	4.2	100			-1.02	-0.74	0.23	0.62	-1.99	A61	Z
23/11/1988	4.2	128			-0.92	-0.68	0.23	0.51	-2.03	A11	Z
23/11/1988	4.2	202			-1.20	-0.24	0.23	0.57	-1.68	DPQ	Z
23/11/1988	4.2	232			-1.24	-0.96	-0.48	-0.28	-2.38	EBN	Z
23/11/1988	4.2	315			-1.26	-0.92	-0.82	-0.72	-2.59	GSQ	Z
23/11/1988	4.2	347			-1.54	-0.89	-0.21	-0.16	-2.29	MNT	Z
23/11/1988	4.2	390			-1.42	-0.49	0.20	-0.16	-1.92	GRQ	Z
23/11/1988	4.2	460			-1.41	-0.62	-0.28	-0.42	-2.29	OTT	Z
23/11/1988	4.2	468			-1.51	-0.80	-0.43	-0.55	-2.48	WBO	Z
23/11/1988	4.2	474			-1.54	-1.30	-1.03	-1.04	-2.89	GGN	Z
06/11/1997	4.5	106	-2.59	-1.79	-0.97	-0.32	0.15	0.58		A11	EHE
06/11/1997	4.5	106	-2.71	-1.77	-1.02	-0.29	0.26	0.43		A11	EHN
06/11/1997	4.5	107	-2.76	-1.91	-1.30	-0.54	0.41	0.87		A54	EHE
06/11/1997	4.5	131	-2.23	-1.33	-0.65	0.09	0.55	0.57		A16	EHE
06/11/1997	4.5	131	-2.00	-1.34	-0.77	0.06	0.67	0.59		A16	EHN
06/11/1997	4.5	132	-2.12	-1.40	-0.54	0.05	0.67	0.86		DAQ	EHZ
06/11/1997	4.5	142	-2.16	-1.36	-0.72	0.22	0.33	0.63		A61	EHE
06/11/1997	4.5	142	-2.40	-1.51	-0.80	0.06	0.35	0.62		A61	EHN
06/11/1997	4.5	163	-2.59	-1.76	-1.11	-0.42	0.20	0.35		A64	EHE
06/11/1997	4.5	163	-2.79	-1.88	-1.14	-0.40	-0.08	0.36		A64	EHN
06/11/1997	4.5	165	-2.55	-1.73	-1.12	-0.45	0.37	0.54		A21	EHE
06/11/1997	4.5	165	-2.76	-1.83	-1.28	-0.53	0.44	0.42		A21	EHN
06/11/1997	4.5	224	-3.06	-1.95	-1.36	-0.74	-0.06	0.20		MNT	EHZ
06/11/1997	4.5	336	-2.62	-1.67	-1.22	-0.61	-0.05	-0.03		GAC	BHE
06/11/1997	4.5	336	-2.85	-1.96	-1.50	-0.73	-0.45	-0.30		GAC	BHN
06/11/1997	4.5	336	-3.10	-2.02	-1.40	-0.87	-0.28	-0.15		GAC	EHZ
06/11/1997	4.5	360	-3.07	-2.17	-1.63	-0.85	-0.51	-0.44		WBO	EHZ
06/11/1997	4.5	367	-3.04	-2.13	-1.70	-0.86	-0.47	-0.33		OTT	EHZ
06/11/1997	4.5	373	-3.00	-2.09	-1.53	-0.63	-0.30	-0.22		CNQ	EHZ
06/11/1997	4.5	398	-3.29	-2.04	-1.57	-0.88	-0.65	-0.64		GSQ	EHZ
06/11/1997	4.5	431	-3.27	-2.39	-1.73	-0.89	-0.56	-0.41		ICQ	EHZ
06/11/1997	4.5	458	-3.03	-2.20	-1.43	-0.89	-0.48	-0.31		MNQ	EHZ
06/11/1997	4.5	466	-3.04	-2.06	-1.33	-0.86	-0.48	-0.55		CRLO	EHZ

06/11/1997	4.5	515	-3.21	-2.45	-1.47	-0.99	-0.68	-0.71	SMQ	EHZ
06/11/1997	4.5	517	-2.91	-1.98	-1.47	-1.05	-1.02	-0.65	LMN	BHE
06/11/1997	4.5	517	-3.00	-2.00	-1.34	-1.04	-0.96	-0.75	LMN	BHN
06/11/1997	4.5	640	-3.20	-2.56	-1.81	-1.28	-0.81	-1.03	SADO	BHE
06/11/1997	4.5	640	-2.81	-2.03	-1.49	-0.90	-0.64	-0.84	SADO	BHN
06/11/1997	4.5	783	-3.02	-2.17	-1.51	-1.10	-0.90	-1.22	LG4Q	EHZ
06/11/1997	4.5	949	-2.92	-1.80	-1.29	-0.87	-1.13	-1.25	SCHQ	BHE
06/11/1997	4.5	949	-3.18	-2.38	-1.75	-1.26	-1.25	-1.34	SCHQ	BHN
06/11/1997	4.5	1067	-3.30	-2.53	-2.14	-1.70	-1.43	-1.13	DRLN	BHE
06/11/1997	4.5	1067	-3.11	-2.46	-2.11	-1.78	-1.55	-1.07	DRLN	BHN
06/11/1997	4.5	1358	-3.01	-2.52	-2.17	-2.09	-2.02	-2.22	TBO	EHZ
06/11/1997	4.5	1833	-3.44	-2.63	-2.20	-2.21	-2.38	-2.54	ULM	BHE
06/11/1997	4.5	1833	-2.91	-2.43	-2.03	-1.84	-2.11	-2.21	ULM	BHN
25/09/1998	4.5	369	-1.83	-1.20	-0.68	-0.17	0.18	0.01	SADO	BHE
25/09/1998	4.5	369	-2.01	-1.22	-0.73	-0.46	-0.10	-0.02	SADO	BHN
25/09/1998	4.5	551	-2.30	-1.26	-0.99	-0.44	-0.16	-0.26	CRLO	EHZ
25/09/1998	4.5	573	-2.06	-1.47	-1.00	-0.63	-0.25	-0.44	EEO	EHZ
25/09/1998	4.5	604	-2.23	-1.55	-1.15	-0.52	-0.59	-0.76	GAC	BHE
25/09/1998	4.5	604	-2.26	-1.57	-1.07	-0.56	-0.66	-0.57	GAC	BHN
25/09/1998	4.5	604	-2.22	-1.32	-1.17	-0.57	-0.26	-0.45	GAC	EHZ
25/09/1998	4.5	828	-2.77	-1.94	-1.40	-0.87	-0.84	-1.01	DPQ	EHZ
16/03/1999	4.5	65	-2.36	-1.43	-0.79	-0.35	0.72	0.81	ICQ	EHZ
16/03/1999	4.5	67	-2.41	-1.73	-0.84	-0.25	0.39	1.08	SMQ	EHZ
16/03/1999	4.5	97	-2.44	-1.53	-0.73	-0.13	0.51	0.61	GSQ	EHZ
16/03/1999	4.5	325	-2.59	-1.64	-0.88	-0.49	0.37	-0.03	A21	EHE
16/03/1999	4.5	325	-2.65	-1.68	-1.11	-0.54	0.10	-0.08	A21	EHN
16/03/1999	4.5	327	-2.41	-1.57	-0.65	-0.71	-0.19	-0.06	A64	EHN
16/03/1999	4.5	348	-2.58	-1.64	-0.97	-0.55	-0.10	-0.06	A61	EHE
16/03/1999	4.5	348	-2.61	-1.54	-1.04	-0.79	-0.12	-0.04	A61	EHN
16/03/1999	4.5	360	-2.75	-1.84	-1.09	-0.69	-0.44	-0.47	A16	EHE
16/03/1999	4.5	360	-2.45	-1.54	-0.92	-0.64	-0.19	-0.37	A16	EHN
16/03/1999	4.5	372	-2.94	-1.97	-1.42	-0.91	-0.19	-0.24	LMQ	BHE
16/03/1999	4.5	372	-2.61	-1.57	-1.07	-0.70	-0.15	-0.06	LMQ	BHN
16/03/1999	4.5	383	-2.19	-1.96	-1.43	-1.04	-0.36	-0.27	A54	EHE
16/03/1999	4.5	383	-2.62	-1.64	-0.99	-0.71	-0.28	-0.33	A54	EHN
16/03/1999	4.5	388	-2.49	-1.65	-1.10	-0.62	-0.32	-0.55	A11	EHE
16/03/1999	4.5	388	-2.48	-1.47	-0.83	-0.48	-0.43	-0.64	A11	EHN
16/03/1999	4.5	402	-2.54	-1.88	-1.08	-0.53	0.04	-0.33	DAQ	EHZ
16/03/1999	4.5	438	-2.63	-2.08	-1.68	-1.19	-1.34	-1.04	LMN	BHE
16/03/1999	4.5	438	-2.68	-2.16	-1.40	-1.21	-1.24	-0.91	LMN	BHN
16/03/1999	4.5	577	-2.97	-2.05	-1.40	-1.08	-1.13	-1.18	SCHQ	BHE
16/03/1999	4.5	577	-2.95	-2.21	-1.75	-1.13	-1.11	-1.21	SCHQ	BHN
16/03/1999	4.5	653	-2.53	-1.99	-1.59	-1.33	-1.13	-1.35	MOQ	EHZ
16/03/1999	4.5	691	-2.83	-2.06	-1.59	-0.87	-1.01	-1.18	LG4Q	EHZ
16/03/1999	4.5	711	-2.80	-2.31	-1.89	-1.27	-1.03	-1.19	MNT	EHZ
16/03/1999	4.5	717	-2.72	-2.43	-1.83	-1.04	-1.00	-1.20	TRQ	EHZ
16/03/1999	4.5	779	-2.71	-2.06	-1.47	-1.18	-0.89	-1.30	GRQ	EHZ
16/03/1999	4.5	808	-2.53	-1.86	-1.22	-1.18	-1.05	-1.11	GAC	BHE
16/03/1999	4.5	808	-2.85	-2.12	-1.44	-1.24	-1.23	-0.80	GAC	BHN
16/03/1999	4.5	808	-2.85	-2.04	-1.49	-1.08	-0.85	-1.22	GAC	EHZ

16/03/1999	4.5	844	-2.67	-2.16	-1.70	-1.10	-1.15	-1.35	OTT	EHZ
16/03/1999	4.5	845	-2.54	-2.23	-1.72	-1.33	-1.29	-1.55	WBO	EHZ
16/03/1999	4.5	912	-2.76	-2.03	-1.42	-1.26	-1.20	-1.48	CRLO	EHZ
16/03/1999	4.5	997	-2.58	-2.07	-1.57	-1.22	-1.17	-1.55	EEO	EHZ
16/03/1999	4.5	1103	-2.95	-2.15	-1.59	-1.55	-1.60	-1.89	SADO	BHE
16/03/1999	4.5	1103	-2.95	-2.15	-1.59	-1.55	-1.60	-1.89	SADO	BHE
16/03/1999	4.5	1103	-2.96	-1.90	-1.41	-1.41	-1.49	-1.75	SADO	BHN
16/03/1999	4.5	1103	-2.95	-1.89	-1.41	-1.41	-1.49	-1.75	SADO	BHN
16/03/1999	4.5	1670	-2.91	-2.40	-1.99	-1.83	-2.17	-2.22	TBO	EHZ
16/03/1999	4.5	2044	-2.92	-2.39	-2.13	-2.29	-2.63	-2.66	FCC	BHE
16/03/1999	4.5	2044	-3.35	-2.79	-2.28	-2.38	-2.79	-2.82	FCC	BHN
16/03/1999	4.5	2096	-0.49	-0.57	-0.67	-0.75	-0.72	-0.71	ULM	BHE
16/03/1999	4.5	2096	-1.75	-1.83	-1.95	-1.94	-1.99	-1.97	ULM	BHN
01/01/2000	4.7	23	-0.16	-0.04	0.27	0.87	1.63	1.85	EEO	EHZ
01/01/2000	4.7	147	-2.34	-1.62	-1.17	-0.40	0.45	1.03	CRLO	EHZ
01/01/2000	4.7	229	-2.19	-1.03	-0.66	-0.11	0.34	0.52	SADO	BHE
01/01/2000	4.7	229	-2.29	-1.38	-0.95	-0.57	0.13	0.26	SADO	BHN
01/01/2000	4.7	235	-2.32	-1.34	-1.08	-0.41	0.34	0.67	GRQ	EHZ
01/01/2000	4.7	293	-2.34	-1.76	-1.14	-0.55	0.03	-0.16	GAC	BHE
01/01/2000	4.7	293	-2.60	-1.74	-1.41	-0.72	-0.22	-0.30	GAC	BHN
01/01/2000	4.7	294	-2.33	-2.00	-1.40	-0.75	-0.06	0.12	OTT	EHZ
01/01/2000	4.7	341	-2.39	-1.87	-1.29	-0.42	0.03	-0.03	TRQ	EHZ
01/01/2000	4.7	395	-2.50	-1.82	-1.07	-0.43	-0.19	-0.28	KAPO	BHE
01/01/2000	4.7	395	-2.51	-1.68	-0.91	-0.53	-0.13	-0.25	KAPO	BHN
01/01/2000	4.7	434	-2.84	-2.30	-1.90	-1.05	-0.64	-0.62	MNT	EHZ
01/01/2000	4.7	469	-2.64	-1.57	-1.13	-0.62	-0.11	-0.28	DPQ	EHZ
01/01/2000	4.7	541	-2.87	-2.17	-1.83	-1.16	-0.92	-1.07	MOQ	EHZ
01/01/2000	4.7	592	-2.60	-1.86	-1.40	-0.76	-0.41	-0.71	DAQ	EHZ
01/01/2000	4.7	647	-2.44	-1.75	-1.50	-0.90	-0.81	-0.95	A54	EHE
01/01/2000	4.7	647	-2.52	-1.69	-1.11	-0.60	-0.57	-0.73	A54	EHN
01/01/2000	4.7	654	-2.55	-1.97	-1.49	-0.83	-0.57	-0.77	LMQ	BHE
01/01/2000	4.7	654	-2.55	-1.71	-1.16	-0.47	-0.43	-0.69	LMQ	BHN
01/01/2000	4.7	663	-2.66	-1.65	-1.38	-0.62	-0.71	-0.95	A11	EHE
01/01/2000	4.7	663	-2.33	-1.89	-1.21	-0.61	-0.89	-1.12	A11	EHN
01/01/2000	4.7	673	-2.68	-2.10	-1.68	-0.99	-0.78	-0.93	A61	EHE
01/01/2000	4.7	673	-2.29	-1.76	-1.44	-0.89	-0.75	-0.87	A61	EHN
01/01/2000	4.7	678	-2.47	-1.79	-1.49	-0.82	-0.90	-1.12	A16	EHE
01/01/2000	4.7	678	-2.40	-1.78	-1.36	-0.82	-0.70	-0.97	A16	EHN
01/01/2000	4.7	690	-2.53	-2.04	-1.61	-1.00	-0.84	-1.13	A64	EHE
01/01/2000	4.7	690	-2.18	-1.72	-1.48	-0.85	-0.59	-0.91	A64	EHN
01/01/2000	4.7	703	-2.70	-2.00	-1.56	-0.55	-0.53	-0.83	A21	EHE
01/01/2000	4.7	703	-2.31	-1.78	-1.27	-0.53	-0.59	-0.84	A21	EHN
01/01/2000	4.7	808	-3.14	-2.35	-1.54	-1.00	-1.15	-1.24	TBO	EHZ
01/01/2000	4.7	830	-2.33	-1.71	-1.36	-1.02	-0.85	-1.05	LG4Q	EHZ
01/01/2000	4.7	851	-2.53	-1.99	-1.42	-0.88	-0.89	-1.12	MNQ	EHZ
01/01/2000	4.7	851	-2.67	-2.11	-1.55	-0.96	-0.94	-1.14	CNQ	EHZ
01/01/2000	4.7	910	-2.53	-1.80	-1.50	-0.68	-1.12	-1.31	GSQ	EHZ
01/01/2000	4.7	914	-2.63	-2.10	-1.55	-1.05	-1.10	-1.40	ICQ	EHZ
01/01/2000	4.7	975	-2.46	-2.02	-1.66	-1.07	-1.07	-1.40	SMQ	EHZ
01/01/2000	4.7	1031	-3.28	-2.67	-1.75	-1.42	-1.46	-1.78	SOLO	EHZ

01/01/2000	4.7	1088	-2.95	-2.37	-2.18	-1.92	-2.13	-2.29		LMN	BHE
01/01/2000	4.7	1088	-2.76	-1.97	-1.99	-1.69	-2.10	-2.14		LMN	BHN
01/01/2000	4.7	1227	-2.66	-2.00	-1.73	-1.56	-1.67	-1.84		SCHQ	BHE
01/01/2000	4.7	1227	-2.64	-2.06	-1.60	-1.35	-1.55	-1.76		SCHQ	BHN
01/01/2000	4.7	1301	-3.34	-2.57	-1.87	-1.60	-2.01	-2.13		ULM	BHE
01/01/2000	4.7	1301	-2.94	-2.00	-1.55	-1.19	-1.57	-1.70		ULM	BHN
01/01/2000	4.7	1665	-2.91	-2.18	-1.82	-1.95	-2.27	-2.34		FCC	BHE
01/01/2000	4.7	1665	-2.71	-2.19	-1.84	-1.94	-2.22	-2.31		FCC	BHN
20/04/2002	5.0	73	-1.21	-0.47	0.05	0.63	1.19	1.57		NCB	BHE
20/04/2002	5.0	73	-1.36	-0.51	0.18	0.76	1.26	1.44		NCB	BHN
20/04/2002	5.0	110	-1.66	-1.00	-0.36	-0.42	-0.31	-0.25		MNT	BHE
20/04/2002	5.0	110	-0.87	-0.95	-0.67	-0.63	-0.25	-0.15		MNT	BHN
20/04/2002	5.0	135	-1.38	-0.48	0.31	0.53	1.39	1.31		WBO	EHZ
20/04/2002	5.0	144	-1.47	-0.76	-0.06	0.35	0.73	0.92		LBNH	BHE
20/04/2002	5.0	144	-1.53	-0.85	0.07	0.37	0.80	0.97		LBNH	BHN
20/04/2002	5.0	144	-1.34	-0.55	-0.01	0.14	0.94	0.94		MOQ	EHZ
20/04/2002	5.0	186	-1.35	-0.58	0.09	0.23	0.85	0.84		OTT	EHZ
20/04/2002	5.0	192	-1.65	-0.87	-0.05	0.39	1.11	1.32		GAC	BHE
20/04/2002	5.0	192	-1.55	-0.71	0.07	0.50	1.05	1.33		GAC	BHN
20/04/2002	5.0	192	-1.34	-0.39	0.19	0.10	0.58	0.70		GAC	EHZ
20/04/2002	5.0	201	-1.43	-0.73	-0.59	-0.02	0.44	0.48		TRQ	EHZ
20/04/2002	5.0	251	-1.81	-1.24	-0.66	-0.37	0.38	0.39		DPQ	EHZ
20/04/2002	5.0	280	-1.67	-0.91	-0.39	0.35	0.21	-0.13		HRV	BHE
20/04/2002	5.0	280	-1.71	-0.99	-0.40	-0.15	0.27	-0.10		HRV	BHN
20/04/2002	5.0	287	-1.64	-1.35	-0.53	0.16	0.28	0.39		GRQ	EHZ
20/04/2002	5.0	316	-1.57	-0.71	-0.39	0.07	0.39	0.24		BINY	BHE
20/04/2002	5.0	316	-1.59	-0.72	-0.45	0.04	0.39	0.24		BINY	BHN
20/04/2002	5.0	334	-1.48	-0.88	-0.54	-0.25	0.27	0.15		CRLO	EHZ
20/04/2002	5.0	839	-2.35	-1.72	-0.75	-0.33	0.03	-0.43		AAM	BHE
20/04/2002	5.0	839	-2.52	-1.37	-0.57	-0.28	-0.03	-0.48		AAM	BHN
20/04/2002	5.0	897	-2.13	-1.56	-0.82	-0.67	0.09	-0.31		ACSO	BHE
20/04/2002	5.0	897	-1.98	-1.36	-0.70	-0.57	0.11	-0.24		ACSO	BHN
20/04/2002	5.0	987	-2.10	-1.29	-0.84	-0.33	-0.43	-0.54		BLA	BHE
20/04/2002	5.0	987	-2.09	-1.29	-0.59	-0.21	-0.28	-0.38		BLA	BHN
20/04/2002	5.0	1373	-2.25	-1.60	-1.35	-1.48	-1.57	-1.61		MYNC	BHE
20/04/2002	5.0	1373	-2.16	-1.84	-1.44	-1.57	-1.67	-1.81		MYNC	BHN
2001India	7.7	166			1.78	1.90		2.08	1.88		
2001India	7.7	216			1.34	1.90		2.01	1.81		
2001India	7.7	150			1.51	1.89		1.99	1.79		
2001India	7.7	225			1.43	1.67		1.73	1.53		
2001India	7.7	44			2.34	2.74		2.87	2.67		
2001India	7.7	147			1.79	2.31		2.52	2.32		
2001India	7.7	238			1.75			2.02	1.82		
2001India	7.7	53			2.11	2.41		2.52	2.32		
2001India	7.7	97			2.16	2.41		2.48	2.28		
2001India	7.7	266			0.95	2.06		2.28	2.08		
2001India	7.7	238			1.82	1.96		2.06	1.86		
2001India	7.7	188			1.43	1.78		1.91	1.71		
2001India	7.7	207			1.65	1.85		1.86	1.66		
2001India	7.7	288			1.17	1.59		1.74	1.54		

Appendix A: EXSIM, a stochastic finite fault modeling program introducing the concept of dynamic corner frequency

(extracted from Motazedian and Atkinson, 2005)

The stochastic model is a commonly used tool for ground motion simulation. The method models ground motion as band limited Gaussian noise, whose amplitude spectrum is given by a seismological model (Boore, 1983). The most commonly-used seismological model for stochastic simulations has been the Brune (1970, 1971) point source model (e.g. Toro et al., 1997). However, point source models are inappropriate for large earthquakes. The effects of a large finite source, including fault geometry, heterogeneity of slip on the fault plane and directivity, can profoundly influence the amplitudes, frequency content and duration of ground motion. Finite-fault effects in ground motions become important for earthquakes with magnitudes exceeding approximately 6.0.

Finite fault modeling has been an important tool for the prediction of ground motion near the epicenters of large earthquakes (Hartzell, 1978; Irikura, 1983; Joyner and Boore, 1986; Heaton and Hartzell, 1986; Somerville et al., 1991; Tumarkin and Archuleta, 1994; Zeng et al., 1994; Beresnev and Atkinson, 1998a). One of the most useful methods to simulate ground motion for a large earthquake is based on the simulation of a number of small earthquakes as subfaults that comprise a big fault. A large fault is divided into N subfaults and each subfault is considered as a small point source (introduced by Hartzell, 1978). The rupture spreads radially from the hypocenter. In our implementation, the ground motions of subfaults, each of which are calculated by the stochastic point-source method, are summed with a proper delay time in the time domain to obtain the ground motion from the entire fault, a(t):

$$a(t)= \sum_{i=1}^{nl} \sum_{j=1}^{nw} a_{ij}(t+\Delta t_{ij}) \qquad (1)$$

where *nl* and *nw* are the number of subfaults along the length and width of main fault, respectively (*nl*nw* = N), Δt_{ij} is the relative delay time for the radiated wave from the ijth subfault to reach the observation point. The $a_{ij}(t)$ are each calculated by the stochastic point source method. The acceleration spectrum for a subfault at a distance R_{ij} is modeled as a point source with an ω^2 shape (Aki, 1967; Brune, 1970; Boore 1983). The acceleration spectrum of shear wave of the ijth subfault, $A_{ij}(f)$, is:

$$A_{ij}(f)=CM_{0ij}(2\pi f)^2/\left[1+(f/f_{0ij})^2\right]\exp(-\pi f\kappa)\exp(-\pi f R/Q\beta)/R_{ij} \qquad (2)$$

where M_{0ij}, f_{0ij} and R_{ij} are the ijth subfault seismic moment, corner frequency and distance from the observation point, respectively. Corner frequency, f_{0ij}, is given by f_{0ij}=4.9e+6 $\beta(\Delta\sigma / M_{0ij})^{1/3}$ where $\Delta\sigma$ is stress drop in bars M_{0ij} is in dyne-cm and β is shear wave velocity in km/s. The constant $C=4\pi^2\Re^{\theta\varphi}/4\pi\rho\beta^3 R_{ij}$, where ρ=density and $\Re^{\theta\varphi}$ = radiation pattern (Boore, 1983). exp (-$\pi f\kappa$) is a high cut filter to model near-surface "*kappa*" effects: this is the commonly-observed rapid spectral decay at high frequencies. The quality factor, *Q*, is inversely related to anelastic attenuation.

The moment of each subfault is controlled by the ratio of its area to the area of the main fault ($M_{oij}=M_o/N$ where M_0 is the seismic moment of the entire fault). If the subfaults are not identical we can express the seismic moment of each subfault as:

$$M_{oij} =(M_o S_{ij})/(\sum_{l=1}^{nl} \sum_{k=1}^{nw} S_{kl}) \quad (3)$$

where S_{ij} is the relative slip weight of the ijth subfault. Earthquake time history simulation deals with the time from the beginning of rupture to the time when the rupture stops. In our finite fault model we deal with a ruptured area that is time dependent; it is initially zero and is finally equal to the entire fault area. Corner frequency is inversely proportional to the ruptured area. Therefore in time history simulation the corner frequency may be considered as a function of time. The rupture begins with high corner frequencies and progresses to lower corner frequencies. We suppose that, during an earthquake, at each moment of time the corner frequency is dependent on the cumulative ruptured area. The rupture history controls the frequency content of the simulated time series.

In our dynamic approach, the corner frequency of the first subfault (near the beginning of rupture) is $f_{011}=S\ 4.9e+6\ \beta\ (\Delta\sigma / M_{011})^{1/3}$, where M_{011} is the seismic moment of the first subfault. The dynamic corner frequency of the ijth subfault, $f_{oij}(t)$, can be defined as a function of $N_R(t)$, the cumulative number of ruptured subfaults at time t:

$$f_{oij}(t)= N_R(t)^{-1/3}\ S\ 4.9e+6\ \beta\ (\Delta\sigma / M_{oave})^{1/3} \quad (4)$$

where $M_{oave} = M_o/ N$ is the average seismic moment of subfaults and S is a constant. As the rupture proceeds towards the end of the fault the number of ruptured subfaults increases and, based on equation 4, the corner frequency of the subfaults decreases. The dynamic corner frequency concept will tend to decrease the high-frequency level of the spectrum of subfaults as the rupture progresses ($A_{ij}(f)_{f>>fijo} \propto f_{oij}^2$). We therefore introduce a scaling factor to conserve the high-frequency spectral level of the radiation produced by each subfault. The acceleration spectrum of the ijth subfault, $A_{ij}(f)$, is thus:

$$A_{ij}(f)=C\ M_{oij}\ H f^2 /[1+(f/f_{oij})^2] \quad (5)$$

$$H_{ij} =(N\Sigma\{f^2/[1+(f/f_0)^2]\} /\Sigma\{f^2/[1+(f/f_{0ij})^2]\})^{1/2} \quad (6)$$

where H is the scaling factor. Thus the diminishing effect of f_{oij} on the high-frequency spectral level from the subfault is compensated for by the scaling factor. The high-frequency spectral contribution from the ijth subfault is equal to that from the first subfault, but the calculation of corner frequency, which controls the shape of the spectrum, comes from the total ruptured area. Consequently, as the rupture progresses there is more low-frequency energy produced, and thus the distribution of energy tends to shift towards lower frequencies.

The new simulation approach is implemented in a modified version of the computer program FINSIM (Beresnev and Atkinson, 1998b). FINSIM is a well-known stochastic finite-fault simulation program that has been validated using data from many earthquakes, including Michoacan, Mexico (1985); Lama Prieta (1989); Northridge (1994); Valparaiso, Chile (1985); and Saguenay, Quebec (1988) (Beresnev and Atkinson

1997, 1998a, 1998b, 1999, 2000, 2001). The modified program has been renamed EXSIM. The modifications include the following features.

- Inclusion of the new concept of "dynamic corner frequency"
- Elimination of multiple triggering of subfaults.
- Variability of pulsing area, or the number of subfaults which are considered as active subfaults in the calculation of dynamic corner frequency. This allows for self-healing slip models.
- Calculation of subfault seismic moment based on dividing the total seismic moment of the earthquake fault by the number of subfaults.

In EXSIM the percentage of pulsing area on the fault will affect the relative amplitudes of low-frequency motion in finite fault modeling. Variation of the stress drop parameter can be used to adjust the relative amplitudes of high-frequency motion. By increasing the stress parameter, the amplitude of high frequencies increases.

A generic EXSIM model was derived by finding the model parameters which best reproduce, on average, the California strong-motion database (as used by Atkinson and Silva, 2000). For this exercise, the regional attenuation parameters used in previous finite-fault simulations for California were adopted (Beresnev and Atkinson, 2001), and the calibration exercise determined the best-fit stress drop and pulsing percentage. These parameters were found to be independent of magnitude, with average values of $\Delta\sigma = 60$ bars and a pulsing percentage of 25%. EXSIM produces similar results to FINSIM over the magnitude range from 5.5 to 7.5, but unlike FINSIM it can be easily extended to smaller magnitudes. The advantage of EXSIM is that it introduces conceptual improvements, such as independence of results from subfault size and conservation of radiated energy, and allows simulation of self-healing slip pulses.

References

Aki, K. (1967). Scaling law of seismic spectrum, J. Geophys. Res. 72, 1217-1231.

Beresnev, I. and G. Atkinson (1997). Modeling finite fault radiation from the w^n spectrum. Bull. Seism. Soc. Am., **87**, 67-84.

Beresnev, I. and G. Atkinson (1998a). Stochastic finite-fault modeling of ground motions from the 1994 Northridge, California earthquake. I. Validation on rock sites. Bull. Seism. Soc. Am., **88**, 1392-1401.

Beresnev, I. and G. Atkinson (1998b). FINSIM - a FORTRAN program for simulating stochastic acceleration time histories from finite faults. Seism. Res. L., **69**, 27-32.

Beresnev, I. and G. Atkinson (1999). Generic finite-fault model for ground motion prediction in eastern North America. Bull. Seism. Soc. Am., **89**, 608-625.

Beresnev, I. and G. Atkinson (2000). Subevent structure of large earthquakes – a ground motion perspective. Geophys. Res. L.,**28**, 53-56.

Beresnev, I. and G. Atkinson (2001). Source parameters of earthquakes in eastern and western North America based on finite-fault modeling. Bull. Seism. Soc. Am., **91**, submitted.

Boore, D. (1983). Stochastic simulation of high-frequency ground motions based on seismological models of the radiated spectra. Bull. Seism. Soc. Am., **73**, 1865-1894.

Brune, J. (1970). Tectonic stress and the spectra of seismic shear waves from earthquakes. J. Geophys. Res., **75**, 4997-5009.

Brune, J. (1971). Correction. J. Geophys. Res., 76, 5002.

Hartzell, S. (1978). Earthquake aftershocks as Green's functions. Geophys. Res. Letters, **5**, 1-14.

Heaton, T., and S. Hartzell (1986). Source characteristics of hypothetical subduction earthquakes in the Northwestern United States. Bull. Seism. Soc. Am., **76**, 675-708.

Irikura, K. (1983). Semi-empirical estimation of strong ground motions during large earthquakes. Bull. Disaster Prevention Res. Inst., Kyoto Univ., **33**, 63-104.

Joyner, W. and D. Boore (1986). On simulating large earthquakes by Green's function additon of smaller earthquakes. In: Earthquake Source Mechanics. Maurice Ewing Volume 6. Geophys. Monogr. Am. Geophys. Union, **37**, 269-274.

Somerville, P., M. Sen and B. Cohee (1991). Simulations of strong ground motions recorded during the 1985 Michoacan, Mexico and Valparaiso, Chile, earthquakes. Bull. Seism. Soc. Am., **81**, 1-27.

Toro, G., N. Abrahamson and J. Schneider (1997). Model of strong ground motion in eastern and central North America: Best estimates and uncertainties. Seism. Res. L., **68**, 41-57.

Tumarkin, A. and R. Archuleta (1994). Empirical ground motion prediction. Annali Di Geofisica. 37, 1691-1720.

Zeng, Y., J. Anderson and G. Yu (1994). A composite source model for computing realistic synthetic strong ground motions. Geophys. Res. L., in press.